

RESEARCH

Open Access



Enhanced anticancer efficacy of oxaliplatin-loaded PEGylated niosomes in breast cancer treatment

Nastaran Asghari Moghaddam^{1*†}, Azadeh Mohammadgholi^{1*†}, Fatemeh Mojtahedi², Niyayesh Akhtari³, Nasim Kaveh Farsani⁴ and Hassan Noorbazargan⁵

[†]Nastaran Asghari Moghaddam and Azadeh Mohammadgholi have contributed equally to this work.

*Correspondence: nas.asgharimoghaddam@iauctb.ac.ir; a.mohammadgholi@yahoo.com

¹ Department of Biology, Central Tehran Branch, Islamic Azad University, Tehran, Iran

² Department of Immunology, Shahid Sadoughi University of Medical Sciences, Yazd, Iran

³ Department of Biology, Faculty of Sciences, Parand Branch of Tehran Azad University, Tehran, Iran

⁴ Department of Chemical Engineering, Isfahan University of Technology, Isfahan 84156-83111, Iran

⁵ Department of Biotechnology, School of Advanced Technologies in Medicine, Shahid Beheshti University of Medical Sciences, Tehran, Iran

Abstract

Breast cancer remains to be one of the most prevalent cancers in women, requiring enhanced treatment approaches. This research improved the formulation of oxaliplatin-loaded PEGylated niosomes with a Central Composite Design (CCD) focused on particle size and drug entrapment efficiency (EE). The antitumor efficacy of the improved niosomes was assessed *in vitro* utilizing MCF-7 breast cancer cells. Furthermore, oxidative stress responses were evaluated, including changes in enzymatic antioxidant defense mechanisms (superoxide dismutase and catalase) and indicators of lipid peroxidation (malondialdehyde and reactive oxygen species levels). The niosomes demonstrated remarkable stability for 2 months at 4 °C, along with pH-dependent drug release. Cytotoxicity experiments demonstrated that PEGylated oxaliplatin-loaded niosomes (PEG-Nio-OXA) exhibited biocompatibility with human foreskin fibroblasts (HFF) while markedly decreasing MCF-7 cell survival. Gene expression study indicated that PEG-Nio-OXA and oxaliplatin-loaded niosomes (Nio-OXA) enhanced pro-apoptotic markers (Bax, caspase-3, caspase-9) while suppressing anti-apoptotic and metastasis-related indicators (Bcl2, MMP-2, and MMP-9). Furthermore, Nio-OXA administration increased oxidative stress, as seen by increased malondialdehyde (98 µM) and reactive oxygen species (ROS) levels while also elevating the enzymatic activity of superoxide dismutase (90 U/mL) and catalase (90 U/mL). Migration experiments verified reduced cellular motility post-treatment. The results indicate that PEG-Nio-OXA is a potential delivery strategy for oxaliplatin in breast cancer treatment.

Keywords: Oxaliplatin, Functionalization, Niosome, Breast cancer, pH-dependent release

Introduction

Breast cancer is currently one of the most commonly diagnosed malignancies and the reason for death among women in the world (Babaei *et al.* 2014; Mansoori-Kermani *et al.* 2022). There are different methods to treat breast cancer, such as chemotherapy, surgery, radiation therapy (RT), targeted therapy, and endocrine (hormone) therapy (ET) (Moghaddam *et al.* 2022). Despite the advantages of chemotherapeutic treatment, the



© The Author(s) 2025. **Open Access** This article is licensed under a Creative Commons Attribution-NonCommercial-NoDerivatives 4.0 International License, which permits any non-commercial use, sharing, distribution and reproduction in any medium or format, as long as you give appropriate credit to the original author(s) and the source, provide a link to the Creative Commons licence, and indicate if you modified the licensed material. You do not have permission under this licence to share adapted material derived from this article or parts of it. The images or other third party material in this article are included in the article's Creative Commons licence, unless indicated otherwise in a credit line to the material. If material is not included in the article's Creative Commons licence and your intended use is not permitted by statutory regulation or exceeds the permitted use, you will need to obtain permission directly from the copyright holder. To view a copy of this licence, visit <http://creativecommons.org/licenses/by-nc-nd/4.0/>.

use of chemotherapeutic approaches has been faced with several restrictions including their toxicity, gastrointestinal upset, bone marrow suppression, and most importantly, drug resistance (Luqmani 2005; Trüeb 2009). Furthermore, antitumor agents used in the treatment of breast cancer have some specific problems, such as poor aqueous solubility, maintenance time in the body and low serum bioavailability, low absorption, and hepatic eradication due to their hydrophobicity properties, which have limited the development of drug candidates from the bench to the bedside (Sanchez-Munoz et al. 2008; Williams et al. 2013). Therefore, new drug delivery systems—such as niosomes—are introduced as thriving techniques as they proliferate the amount of drug penetration, enhance tumor-targeting, and minimize drug side effects (Karimifard et al. 2022; Mahdizadeh et al. 2024). Niosomes are nano-sized vesicles comprised of nonionic surfactants and cholesterol (Amoozegar et al. 2022; Mehrarya et al. 2022; Wiranowska et al. 2020; Dabbagh Moghaddam et al. 2021). Oxaliplatin (*trans*-L-diamino cyclohexane oxalate platinum), L-OXA is introduced as the third generation of platinum classic platinum-based anticancer drugs after cisplatin and carboplatin. Oxaliplatin as a cisplatin derivative has shown that it has a wide *in vitro* and *in vivo* antitumor effect and can reduce the side effects of cisplatin, such as peripheral neuropathy, which causes severe pain in hands and feet, and kidney toxicity (Kidani et al. 1980; Suzuki et al. 2008; Wiseman et al. 1999). Its mechanisms against tumors are like cisplatin when L-OXA inhibits DNA synthesis by forming DNA adducts. It can also inhibit RNA synthesis unlike cisplatin (Kidani et al. 1980; Riviere et al. 2011). Some investigations have revealed that oxaliplatin is widely used to treat various cancers, e.g., breast cancer. Despite the above-mentioned benefits, oxaliplatin is not without several pharmacokinetic and toxicological challenges (Duncan et al. 2010; André et al. 2009). Therefore, the design of an L-OXA-based drug delivery system using niosomes could reduce the potential side effects, increase specific target organs, and improve the therapeutic effects (Allen and Cullis 2013; Maksimenko et al. 2014; Miyajima et al. 2006; Doi et al. 2019). Niosomes are considered bilayer non-ionic surfactant-based vesicles, which have been widely employed to deliver poorly water-soluble drugs and enhance their dissolution and bioavailability to enhance (Naseroleslami et al. 2022; Bourbour et al. 2022). Niosomes are non-ionic surfactant vesicles with a bilayer structure, so they are like liposomes structurally, but they have more stability and lower cost than liposomes. Furthermore, like liposomes, they can incorporate both hydrophilic and hydrophobic drugs *in their* core and between the bilayers, respectively (Akbarzadeh et al. 2020a, 2020b; Moghtaderi et al. 2021). In addition, several niosomal formulations have been used to carry drugs to cancer cells in ways to minimize side effects on healthy cells as they are sensitive to pH (Akbarzadeh et al. 2020a, 2020c).

Niosomal vesicles, *like* other bilayer vesicular drugs, may exhibit stability problems, including aggregation, drug leakage, and other instability phenomenon during the long-term preservation process, so coating the surface of niosomes with inert polymeric molecules causes them to improve their stability (Sahrayi et al. 2021; Yadavar-Nikravesht et al. 2021). Among these hydrophilic molecules, polyethylene glycol (PEG) polymer is a successful material, which has been used extensively as a surface modifier to stabilize the niosomes. PEG is a synthetic polymer that is highly water-soluble, biocompatible, non-toxic, non-immunogenic, and non-antigenic. Since the modification of niosomes with polymers can increase pharmacological activities and the improvement of therapeutic

effects of various insoluble drugs and bioactive molecules (Cheng et al. 2021; Luciani et al. 2004; Baranei et al. 2021).

This study presents a novel approach to breast cancer treatment by optimizing the formulation of oxaliplatin-loaded niosomes decorated with polyethylene glycol (PEG). Unlike previous studies, our research employs a Central Composite Design (CCD) to achieve optimal particle size and drug loading efficiency, ensuring enhanced stability and targeted delivery. The innovative PEGylated niosomal system not only demonstrates significant cytotoxicity against MCF-7 breast cancer cells but also exhibits pH-dependent release behavior, superior antioxidant activity, and effective inhibition of cell migration. These findings underscore the potential of PEG-Nio-OXA as a promising nanocarrier for improving the therapeutic efficacy of oxaliplatin in breast cancer treatment.

Materials and methods

For detailed methods see SI.

Results and discussion

Fabrication and optimization

Effect of oxaliplatin: lipid and Span 60:Tween 60 on size

The independent variables (low, medium, and high levels) are presented in Table S1. The vesicle size of oxaliplatin niosomes ranged from 165.5 (F9) to 289.1 nm (F11), as shown in Table 1. The analysis of variance for particle size is listed in Table 2. The best-fitted model for particle size was quadratic and significant ($p < 0.05$). The Tween 60 to Span 60 ratio (B) significantly influences particle size, as seen by the ANOVA data. The prominent quadratic component (B^2) underscores a substantial non-linear effect. Nonetheless, the lipid-to-drug ratio (A) and its quadratic effect (A^2) do not have a substantial influence on size. The negligible combined effects on particle size are evidenced by

Table 1 Design of experiments using the CCD method to optimize the niosomal formulation of oxaliplatin

Run	Levels of independent variables		Dependent variables		
	Lipid:drug (mol ratio)	Span 60:Tween 60 (mol ratio)	Average size (nm)	PDI	Entrapment efficiency (EE) (%)
1	0	-1	270.6	0.315	53.19
2	-1	0	197.5	0.317	61.42
3	1	1	231.7	0.307	72.34
4	0	0	174.3	0.229	68.21
5	1	0	200.2	0.220	69.25
6	-1	1	211.6	0.284	58.49
7	0	1	227.7	0.205	62.35
8	0	0	168.3	0.248	66.45
9	0	0	165.5	0.220	67.09
10	-1	-1	254.2	0.382	53.21
11	1	-1	289.1	0.273	60.49

The table includes the independent variables (lipid-to-drug ratio and Span 60:Tween 60 ratio) and their corresponding effects on the dependent variables, namely, average particle size (nm), polydispersity index (PDI), and entrapment efficiency (EE, %)

Table 2 Analysis of variance for the quadratic polynomial model for particle size

Source	p value	Evaluation
Model	0.003	Significant
A	0.140	
B	0.007	
AB	0.606	
A ²	0.195	
B ²	0.000	

This table presents the analysis of variance (ANOVA) results for the quadratic polynomial model, evaluating the effects of independent variables on the particle size of niosomal formulations

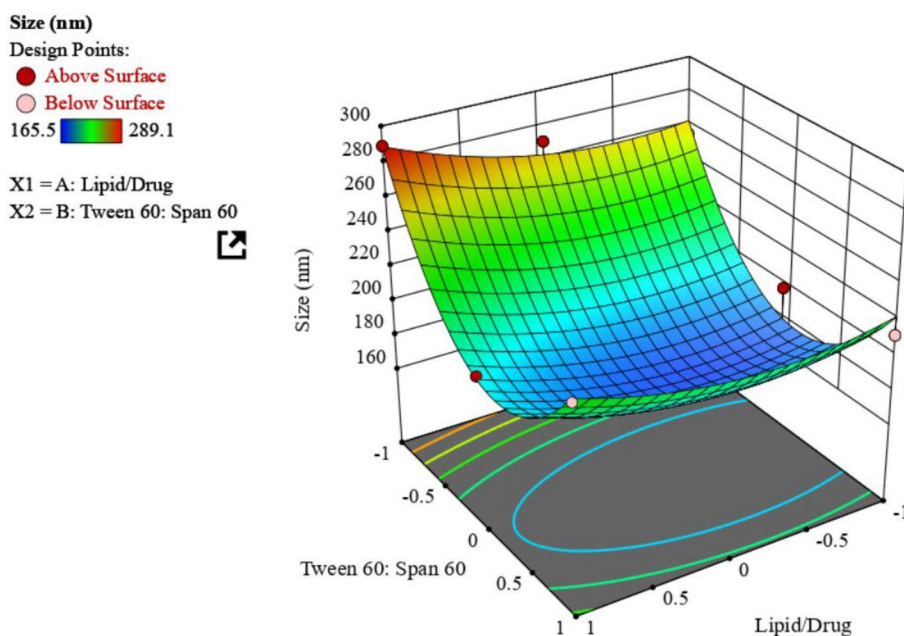


Fig. 1 CCD response surface plot for particle size as a function of lipid-to-drug and Tween 60:Span 60 ratios. This 3D response surface plot, generated using Design-Expert® software, illustrates the effects of the lipid-to-drug ratio (X1) and Tween 60:Span 60 ratios (X2) on the particle size (nm) of niosomal formulations. The plot visualizes how these independent variables influence the size of the particles, with size values represented by a color gradient ranging from 165.5 nm (blue) to 289.1 nm (red)

the non-significant interaction between A and B (AB). The particle size equation demonstrates the impact of the lipid-to-drug ratio (A) and the Span 60:Tween 60 ratio (B) on niosomal formulation size, encompassing their interaction and quadratic effects. An elevated lipid-to-drug ratio results in a marginal rise in particle size, as seen by A’s positive coefficient, whereas B’s negative coefficient indicates that augmenting the Span 60:Tween 60 ratio diminishes particle size. The interaction term AB (Table S2) indicates a negligible joint influence of A and B on size. The resulting equations in terms of coded value were as follows:

$$\text{Size} = +176.10 + 9.62 * A - 23.82 * B - 3.70 * AB + 12.65 * A^2 + 62.95 * B^2$$

3D contour plots (Fig. 1) have been used to illustrate how independent variables affect size. The size of niosomes increases as lipid:drug concentration (A) rises. The response

surface figure highlights important patterns in the connection between the lipid-to-drug ratio (X1) and the Tween 60:Span 60 ratios (X2), showing how these factors affect the particle size of niosomal formulations. The best lipid-to-drug and Tween 60:Span 60 ratio combinations result in the lowest particle sizes (~165.5 nm, blue regions). By stabilizing the bilayer structure, increasing the lipid-to-drug ratio first decreases particle size (Daeihamed *et al.* 2017); however, too much lipid causes aggregation and higher particle sizes (~289.1 nm, red regions). By supplying enough lipid material to create stable bilayers, a moderate lipid-to-drug ratio encourages smaller particle sizes. However, aggregation and the creation of multi-lamellar vesicles take place when the lipid content surpasses the ideal threshold, leading to an increase in particle size. Like this, an ideal Tween 60:Span 60 ratio reduces particle size by preserving a balanced hydrophilic–lipophilic profile, whereas larger and less stable particles are the consequence of surfactant composition imbalances (Durak *et al.* 2020). The way these factors interact shows that exact optimization is crucial to achieving the smallest particle sizes. The hydrophilic–lipophilic balance of the surfactants is modulated by the Tween 60:Span 60 ratio, which has a considerable impact on particle size. While deviations from this equilibrium result in structural instability and greater particle sizes, a balanced ratio stabilizes the bilayer and reduces particle size. The findings demonstrate that lowering particle size and improving the homogeneity of niosomal formulations require maintaining an ideal Tween 60:Span60 ratio. An increase in the amount of lipid concentration has a linear relation with the vesicle size. However, the particle size of niosomes reduces with the increase in the Span 60:Tween 60 ratio. The increase in span 60 concentration results in the higher solubility of oxaliplatin, which may lead to a decrease in the size of the vesicle (Mohanty *et al.* 2020). Lipids can enter the lipid bilayer by their hydrophobicity character. As a result, the vesicular membrane becomes disordered, and the structure becomes more thermodynamically stable as the radius of the molecules increases (Essa 2010).

The ratios of Tween 60 to Span 60 and lipid-to-drug are essential in defining niosome size, since they influence bilayer stability, packing efficiency, and membrane fluidity. In addition to Tween 60 to Span 60 produces bigger niosomes, since the hydrophilic characteristics of Tween 60 interfere with the dense arrangement of Span 60, hence improving membrane fluidity and steric hindrance (Bnyan *et al.* 2018). Tween 60 about Span 60 produces bigger niosomes, since the hydrophilic characteristics of Tween 60 interfere with the dense arrangement of Span 60, hence improving membrane fluidity and steric hindrance (Pando Rodríguez 2014). This results in bilayer expansion and water infiltration, leading to vesicle swelling. In contrast, an elevated Span 60 concentration yields smaller, more rigid vesicles owing to its reduced HLB value, hence enhancing bilayer stability (Basiri *et al.* 2017). The lipid-to-drug ratio strongly influences vesicle size. An increased lipid-to-drug ratio enhances bilayer stability, diminishes vesicle fusion, and inhibits excessive swelling, leading to smaller, more stable vesicles (Bulbake *et al.* 2017; Tang *et al.* 2023). A diminished lipid-to-drug ratio may destabilize the bilayer due to drug-induced perturbations, resulting in bigger vesicles.

Effect of oxaliplatin: lipid and Span 60:Tween 60 on polydispersity index (PDI)

The PDI of all niosome formulations obtained by central composite design (CCD) ranged from 0.205 to 0.382 (Table 1). In the model fit for the polydispersity index

of niosomes, the sequential *p* value of the linear model was estimated to be 0.023. The ANOVA findings for the *p* values show that the Tween 60:Span 60 ratio (*B*) and the lipid-to-drug ratio (*A*) have a substantial impact on the formulations' PDI, underscoring their crucial roles in maintaining particle size uniformity. However, are not statistically significant, indicating that their combined and non-linear effects do not affect the PDI (Table 3). Based on Table 3, all independent variables except *AB* and *B*² models have a significant effect on PDI (*p* < 0.05). The influence of formulation factors on size uniformity is demonstrated by the polydispersity index (PDI) equation. A negative coefficient for *A* signifies that size homogeneity is enhanced by reducing PDI via an elevation in the lipid-to-drug ratio. Similarly, *B* reduces PDI, emphasizing the need of optimal Span 60:Tween 60 ratios. The interaction term *AB*, when *A* and *B* are coupled, results in a little rise in PDI, indicating potential variability. The relationship between PDI and independent variables is presented by the following regression equation:

$$PDI = +0.23 - 0.031 * A - 0.029 * B + 0.033 * AB + 0.044 * A^2 + 0.036 * B^2$$

According to Table S3 for the regression and Fig. 2, the Tween 60:Span 60 ratios (X2) and the lipid-to-drug ratio (X1) affect the polydispersity index (PDI) of niosomal formulations, emphasizing how important these factors are for particle size uniformity. The most uniform particle sizes are represented by PDI values of about 0.205 in the yellow regions, while larger variability is shown by PDI values of 0.382 in the blue regions. Since increasing the amount of Span 60 results in a decrease in particle size, the accumulation of smaller niosomes that were present during the dispersion has led to a decrease in the PDI (Basiri et al. 2017). According to previous studies, the addition of lipids leads to produce rigid, stable, and intact niosomal structures that show low PDI value. However, niosomes have a gel-like structure in the absence of lipids (Khan et al. 2019). The niosomal bilayer's stability is greatly aided by the Tween 60:Span 60 ratio. A stable bilayer structure that minimizes PDI and decreases size fluctuation is produced by striking an ideal balance between hydrophilic and lipophilic characteristics. The integrity of the bilayer is compromised by imbalances in this ratio, on the other hand, which results in increased particle size heterogeneity. When the Tween 60:Span 60 ratio and the lipid-to-drug ratio are tuned within certain limits, the lowest PDI values (~0.205) are obtained.

Table 3 Analysis of variance for the quadratic polynomial model for Polydispersity Index (PDI)

Source	<i>p</i> value	Evaluation
Model	0.024	Significant
<i>A</i>	0.038	
<i>B</i>	0.045	
<i>AB</i>	0.056	
<i>A</i> ²	0.046	
<i>B</i> ²	0.086	

This table presents the analysis of variance (ANOVA) results for the quadratic polynomial model used to evaluate the effects of independent variables on the polydispersity index (PDI) of niosomal formulations

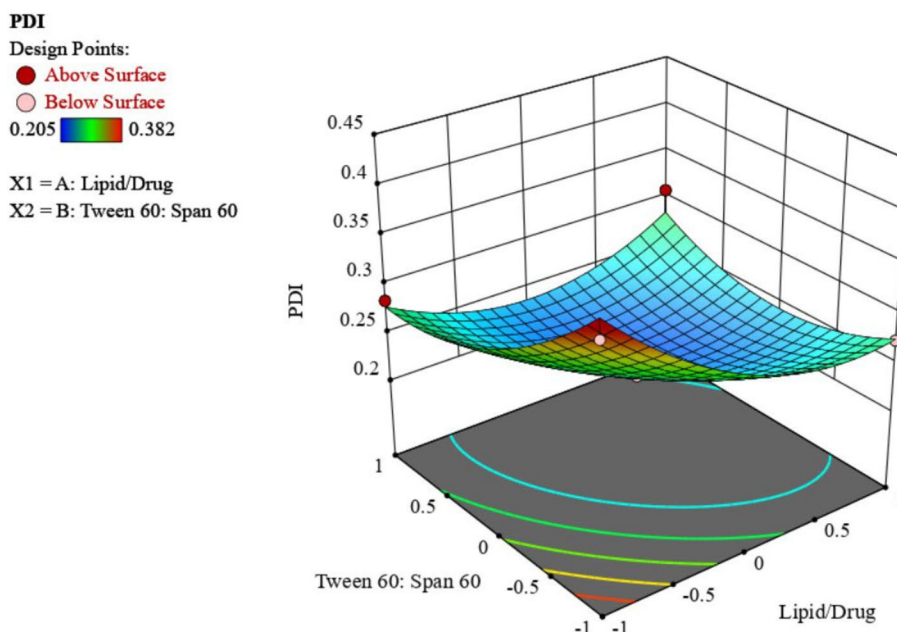


Fig. 2 CCD response surface plot for PDI as a function of lipid-to-drug and Tween 60:Span 60 ratios. This 3D response surface plot illustrates the effects of two independent variables—lipid-to-drug ratio (X1) and Tween 60:Span 60 ratio (X2)—on the polydispersity index (PDI) of niosomal formulations, as predicted by the Central Composite Design (CCD) model. The PDI values, which reflect the size uniformity of the particles, are represented by a color gradient ranging from yellow (lowest PDI ~0.205) to blue (highest PDI ~0.382)

Table 4 Analysis of variance for the quadratic polynomial model for EE

Source	p value	Evaluation
Model	0.003	Significant
A	0.002	
B	0.003	
AB	0.176	
A ²	0.539	
B ²	0.003	

This table presents the analysis of variance (ANOVA) results for the quadratic polynomial model used to evaluate the effects of independent variables on the EE of niosomal formulations

Effect of oxaliplatin: lipid and Span 60:Tween 60 on entrapment efficiency (EE%)

Table 1 shows the summary of EE% of oxaliplatin from niosomes. High entrapment efficiency is the percentage fraction of total oxaliplatin entrapped into the nanocarriers. The maximum entrapment efficacy obtained for oxaliplatin was 72.34%. These results show that both elements independently contribute significantly to increasing EE%, with the Tween 60:Span 60 ratio improving bilayer stability through a balanced hydrophilic–lipophilic interaction and the ideal lipid-to-drug ratio providing adequate bilayer volume for drug encapsulation. Furthermore, the Tween 60:Span 60 ratio (B2) quadratic effect was statistically significant, indicating that optimizing EE% requires precise surfactant composition (Table 4). However, the quadratic effect of the lipid-to-drug ratio and the interaction between A and B were not significant, suggesting that their combined or non-linear effects do not significantly add to the

model. The regression equations of EE% for oxaliplatin are presented in Table S4. The effect of formulation variables on drug encapsulation is reflected in the entrapment efficiency (EE) equation. A and B have positive coefficients, suggesting that EE is enhanced by greater lipid-to-drug and Span 60:Tween 60 ratios. Combining these variables further enhances encapsulation, albeit to a lesser degree, as indicated by the interaction term *AB*:

$$EE = +66.14 + 4.83 * A + 4.38 * B + 1.64 * AB + 0.86 * A^2 - 6.70 * B^2$$

The effects of the Tween 60:Span 60 ratio (X2) and the lipid-to-drug ratio (X1) on the entrapment efficiency (EE%) of niosomal formulations are depicted in the 3D response surface plot (Fig. 3). The crucial impact of these formulation factors is demonstrated by the EE% values, which range from roughly 53.19% in the blue regions to a maximum of 72.34% in the red regions. By supplying more lipid bilayer material to encapsulate the drug, a rise in the lipid-to-drug ratio raises the EE%. However, there comes a point at which further increases in the lipid ratio cause a plateau or minor decrease in efficiency because of a saturation effect. Likewise, the niosomal bilayer is stabilized and drug retention is enhanced by the Tween 60:Span 60 ratio. By improving the hydrophilic–lipophilic balance, higher Tween 60:Span 60 ratios improve encapsulation; however, too high ratios can weaken stability and jeopardize bilayer integrity. The maximum EE% is seen at intermediate values of both the lipid/drug ratio and the Tween 60:Span 60 ratio, indicating a synergistic impact between the two factors. Overall, the findings show that the best Tween 60:Span 60 and lipid/drug ratio combination produces a maximum EE% of roughly 72.34%.

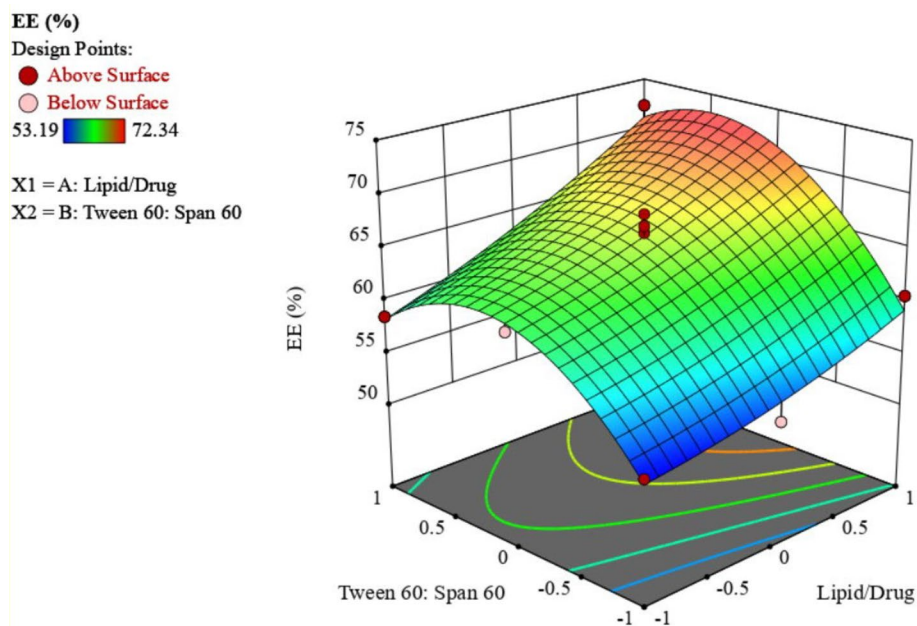


Fig. 3 3D response surface plot for entrapment efficiency (EE%). This 3D surface plot, generated using Design-Expert® software, illustrates the effects of two independent variables—lipid-to-drug ratio (X1) and Tween 60:Span 60 ratio (X2)—on the entrapment efficiency (EE%) of niosomal formulations. The predicted EE% values are displayed as a function of these variables, with the color gradient representing the range of EE% values

The concentration drug: lipid and the ratio Span 60:Tween 60 have a positive effect on EE%. As the concentration of Span 60 increases, % EE also increases. The niosomal membrane became less permeable with increasing the concentration of Span 60. As a result, the percent encapsulation efficiency was promoted along with Increasing Span 60 concentration (Balakrishnan et al. 2009). In addition, the increase of the L/D molar ratio can result in a rise in the concentration of materials used to create bilayers and lead to the expansion of vesicles in a given volume so a rise in the amount of oxaliplatin entrapped in the vesicles is observed (Arzani et al. 2015). Higher lipid-to-drug ratio stabilizes the bilayer, reducing drug leakage and increasing EE%, particularly for lipophilic drugs. Conversely, a low lipid-to-drug ratio results in poor bilayer integrity, increasing permeability and reducing EE%.

Validity of the central composite design (CCD)

Predicted R^2 is measured to show how good response value is predicted. Accordant to the previous study, Adjusted R^2 is in reasonable agreement with predicted R^2 as the ratio of predicted R^2 to adjusted R^2 is less than 0.2. The data of related regression analysis for different responses are presented in Tables S2–4 indicating that there is a reasonable agreement between R^2 and adjusted R^2 . Furthermore, the signal-to-noise ratio is calculated by adequate precision noise, which shows all responses are greater than 4 so design space can be navigated using the model.

Data optimization

By comparing the expected values from Central Composite Design (CCD) with actual data under ideal circumstances, the results shown in Table 5 illustrate the optimized responses for Nio-OXA, Nio-OXA-PEG, and pure niosomes. The CCD model's accuracy was demonstrated by the projected average particle size of 184.6 nm for Nio-OXA, which nearly matched the experimental measurement of 183.1 ± 6.7 nm. As seen in Nio-OXA-PEG (166.4 ± 5.3 nm), PEGylation dramatically decreased the particle size in comparison with Nio-OXA. This was probably caused by the PEG layer's stabilizing effect, which compacted the niosomal structure (Alemi et al. 2018). Since encapsulating oxaliplatin and PEG surface modification were absent, pristine niosomes had the shortest size (135.5 ± 4.3 nm). CCD anticipated that Nio-OXA's polydispersity index (PDI) would be 0.228, while the experimental result was 0.202 ± 0.010 , indicating better-than-expected size uniformity. PEGylation highlighted the stabilizing impact of PEG by further improving the PDI to 0.194 ± 0.011 in Nio-OXA-PEG. Due to their simpler composition

Table 5 Optimized responses predicted by CCD and experimental data for niosomal formulations

Parameter	Predicted by CCD	Experimental Data (Nio-OXA)	Nio-OXA-PEG	Niosome (Nio)
Average size (nm)	184.6	183.1 ± 6.7	166.4 ± 5.3	135.5 ± 4.3
PDI	0.228	0.202 ± 0.010	0.194 ± 0.011	0.172 ± 0.008
Entrapment Efficiency (EE) (%)	70.48	65.41 ± 1.24	70.31 ± 1.62	–

This table presents the optimized responses predicted by the Central Composite Design (CCD) method compared to the experimental data obtained for Nio-OXA and Nio-OXA-PEG formulations under optimum conditions. The parameters analyzed include average particle size, polydispersity index (PDI), and entrapment efficiency (EE%), providing insights into the accuracy of the predictions and the performance of the formulations

without drug encapsulation or surface modification, pristine niosomes had the lowest PDI (0.172 ± 0.008), indicating the maximum consistency. The experimental result for entrapment efficiency (EE%) was $65.41 \pm 1.24\%$, which was within an acceptable range, but CCD predicted a value of 70.48% for Nio-OXA. PEGylation in Nio-OXA-PEG increased EE% to $70.31 \pm 1.62\%$, which was in good agreement with the expected value and validated PEG's contribution to better drug retention (Alemi et al. 2018). PEGylation in Nio-OXA-PEG continuously enhanced performance indicators when comparing the groupings. A decrease in the size of niosomes coated with PEG can be attributed to the affinity between PEG and the bilayer of niosomes. Physical bonding, such as hydrogen bonding between PEG and niosomes, increases the cohesion of niosomes, which leads to a decrease in particle size (Cheng et al. 2021).

Morphological survey of the optimized oxaliplatin-loaded PEGylated niosomes (PEG-Nio-OXA)

The hydrodynamic diameters of the formulations show a gradual rise in size with oxaliplatin loading and PEGylation, according to the DLS analysis (Fig. 4A). The particle size of Nio-OXA grew to 140 nm, indicating the inclusion of oxaliplatin into the niosomal bilayer, whereas that of Pristine Nio was around 120 nm. The size was further enhanced by PEGylation to roughly 150 nm, indicating that the PEG layer had successfully adhered to the niosomal surface. For reproducibility and stability in biological settings, homogeneous particle preparation is indicated by the narrow size distribution for all formulations. The inclusion of the hydration layer and any surface-bound molecules in the hydrodynamic diameter is responsible for the larger size seen in DLS measurements as opposed to scanning electron microscopy (SEM) or transmission electron microscopy (TEM) observations. This highlights the use of DLS in evaluating particle behavior in aqueous systems. SEM image of the optimized formulation which has a spherical morphology with a good size distribution below 100 nm with no bulk component (Fig. 4B). The inherent morphological features of PEG-Nio-OXA are shown in Fig. 4C, which was examined by TEM assessment. The results of TEM showed that the PEG-Nio loaded with OXA had a spherical shape and was discrete without any aggregation or agglomeration. The particle size of samples obtained by SEM/TEM microscopy was smaller than that examined via DLS. Since nanoparticle sizes were determined on hydrated vesicles using the DLS method, measuring the size of samples was carried out in the presence of water, which caused samples to show larger sizes compared to the dry vesicles in SEM/TEM microscopy (Akbarzadeh et al. 2020b, 2021).

Analysis of Fourier transform infrared (FTIR)

Figure 4D shows the chemical structure of Tween 60, span60, cholesterol, naked Niosome, pure Oxaliplatin, Niosome–Oxaliplatin, and PEGylate–Niosome–Oxaliplatin. FTIR spectra for Tween-60 (Fig. 4D-a) show that the band observed at 3435 cm^{-1} substantiated the existence of N–H stretching in 2°-amines. The band seen at 3435 cm^{-1} was attributed to cholesterol and Tween-60 (N–H stretching in 2°-amines vs. O–H Stretching in phenols) and the peak at 1148 cm^{-1} is related to C–O stretching in Tween-60. C–N and C–O stretching is present at 1148 cm^{-1} , which belongs to the Tween-60 range. C–N stretch and C–O stretching occur at 1148 cm^{-1} belonging to Tween-60.

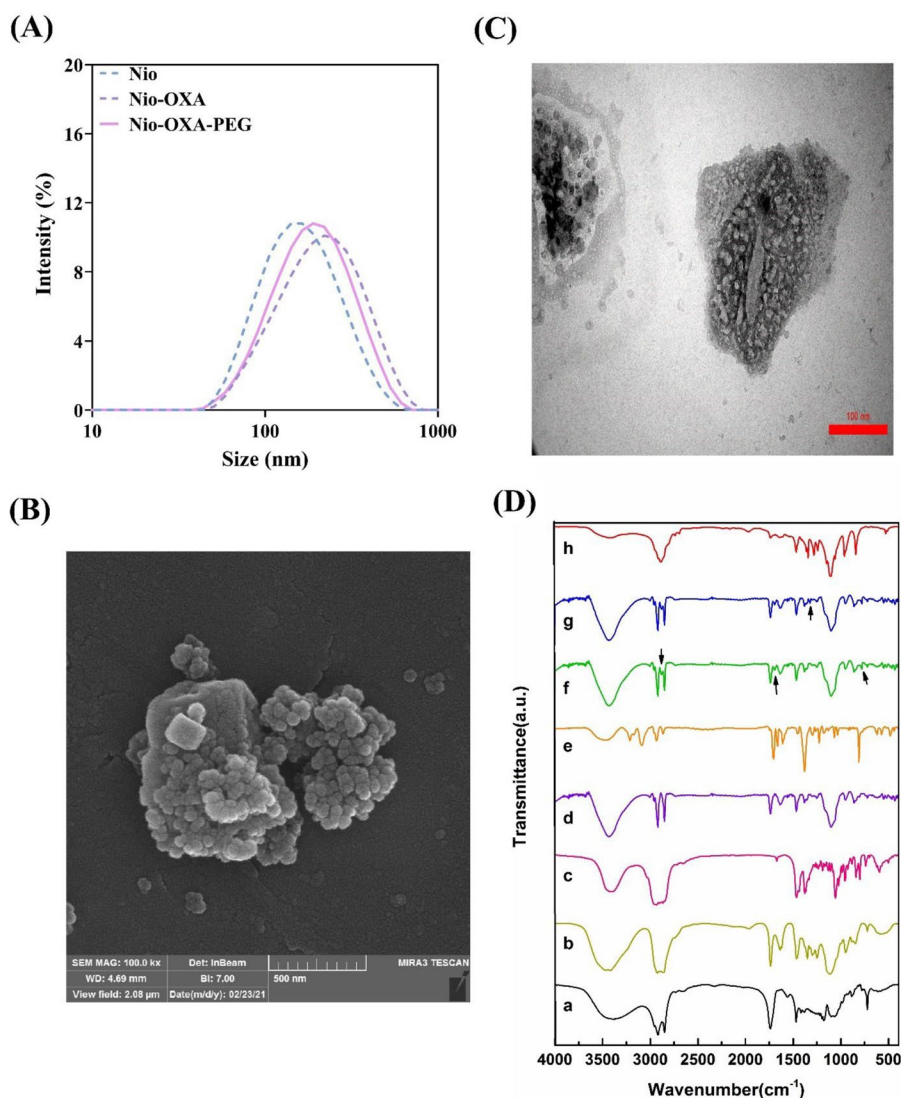


Fig. 4 **A** Dynamic light scattering (DLS); the size distribution of pristine Nio, Nio-OXA, and Nio-OXA-PEG formulations measured in their hydrated state. The hydrodynamic diameters are centered at approximately 120 nm for pristine Nio, 140 nm for Nio-OXA, and 150 nm for Nio-OXA-PEG. **B** Scanning electron microscopy (SEM); the Nio-OXA-PEG appears spherical and smooth, with an average size of 100–120 nm. Slight aggregation is visible due to the drying process during SEM sample preparation. **C** Transmission electron microscopy (TEM); the niosomes exhibit a well-defined core-shell structure, with darker cores indicating oxaliplatin encapsulation and lighter layers representing the PEG coating. The observed size ranges from 100–120 nm, consistent with SEM measurements but smaller than DLS results due to the absence of the hydration layer. **D** Fourier transform infrared (FTIR) Spectroscopy; Spectral analysis of various components and formulations, including a: Tween 60, b: span 60, c: cholesterol, d: niosome, e: oxaliplatin, f: niosome-oxaliplatin, g: nio-Oxaliplatin-PEG, h: PEG

According to Fig. 4D-b for Span 60, the peaks at 2916.75 cm^{-1} , and 2849.58 cm^{-1} were related to OH stretch, broad, and OH stretch, broad, as well as a cyclic 5-membered ring peak at 1734.65 cm^{-1} and small peaks between 1000 and 1200 cm^{-1} was attributed aliphatic groups. The FTIR pattern for cholesterol shows that the wave number of O–H stretching at 3392 cm^{-1} , C–H stretching at 2931 cm^{-1} , C=C stretching at 1458 cm^{-1} , and C–O bending vibrations 1070 cm^{-1} are all depicted in Fig. 4D-c. According to the

Naked niosomes (Fig. 4D-d) showed the characteristic band peak at 1736 cm^{-1} due to C=O stretching vibration. A typical broad peak at 3406 cm^{-1} (O–H stretching) peaks at 1000 to 1292 cm^{-1} due to aliphatic C–N stretching. Oxaliplatin as a pure drug showed the characteristic band peak at 1674 and 1713 cm^{-1} due to the C=O stretching vibration, 3087 cm^{-1} due to N–H stretching, and 813 cm^{-1} due to N–H bending band (Fig. 4D-e). The FTIR pattern for Nio-OXA (Fig. 4D-f) shows that the peak of the C=O group is related to free OXA shifts and observed at 1695 cm^{-1} . In addition, the CH_2 appears at lower wavelengths, which confirms loading Oxaliplatin in niosomes. According to the FTIR spectra of Nio-OXA coated with PEGylate (Fig. 4D-g), C–H bonding and stretching vibrations of carboxylate in PEG shifted to lower wavelengths 1589 and 1316 cm^{-1} , respectively, compared to pristine PEG (Fig. 4D-h) because of chemical bonding between the groups of carboxylate PEG and the Nio-OXA structure.

Drug release and modeling kinetic

The in vitro drug release profile showed free oxaliplatin (OXA) rapid and complete release within 12 h, while Nio-OXA and Nio-OXA-PEG showed sustained release over 72 h, with slower release at pH 5.4 compared to pH 7.4 (Fig. 5A). This pH-sensitive release behavior is especially pronounced for Nio-OXA-PEG, which released less drug at acidic pH, suggesting its potential for targeted delivery in the acidic tumor microenvironment (Safari Sharafshadeh et al. 2024). The sustained release of Nio-OXA and Nio-OXA-PEG, especially at physiological pH, highlights their ability to provide controlled drug delivery, potentially improving therapeutic outcomes while minimizing systemic side effects. These findings are consistent with earlier research that reported slower drug release in pH-responsive systems, enhancing tumor-specific delivery. Free oxaliplatin's (OXA) cumulative drug release was quick, reaching almost 90% in just 8 h, almost 100% in 24 h, and stable for 72 h. Nio-OXA (pH 7.4), on the other hand, released the medication significantly more slowly, with just 21% released at 4 h, 31% at 8 h, and 64% at 72 h. An even slower release profile was also displayed by Nio-OXA-PEG (pH 7.4), which was 15% at 4 h, 25% at 8 h, and 50% at 72 h. A slower release was noted for formulations evaluated at pH 5.4 as opposed to pH 7.4. About 31% of Nio-OXA (pH 5.4) was released at 4 h, 47% after 8, and roughly 80% after 72 h. These findings unequivocally demonstrate the Nio-OXA and Nio-OXA-PEG formulations controlled and sustained release behavior, especially in acidic environments (pH 5.4), which may be useful for addressing the acidic tumor microenvironment. The encapsulation of oxaliplatin within the niosome structure is responsible for the sustained release seen in the Nio-OXA and Nio-OXA-PEG formulations. Drug diffusion is inhibited by niosomes, which are bilayer vesicles made of cholesterol and non-ionic surfactants. The encapsulated medicine can be released gradually over time thanks to this structure, which slows down its release. One of the main benefits of chemotherapy medications is sustained release, which lowers systemic toxicity, decreases the frequency of administration, and helps sustain therapeutic drug levels for a longer period. The drug release profile revealed that release rates were slower at pH 5.4 compared to pH 7.4. This difference can be explained by the stability of the niosome structure in acidic conditions. At acidic pH (5.4), typical of the tumor microenvironment, the bilayer vesicles may experience less swelling or disruption,

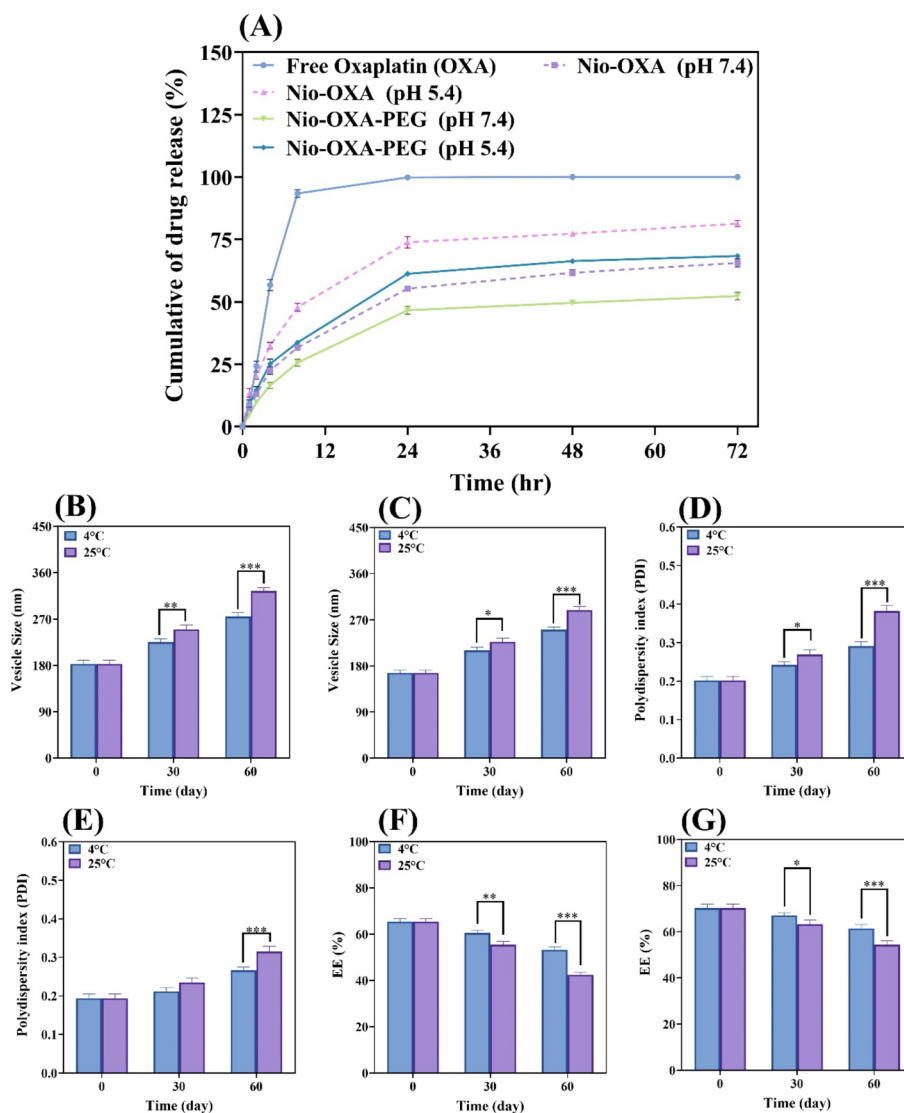


Fig. 5 **A** In vitro drug release profiles: cumulative release of oxaliplatin (OXA) from free OXA, Nio-OXA, and Nio-OXA-PEG formulations under different pH conditions (pH 7.4 and pH 5.4) over 72 h. **B, C** Changes in particle size of Nio-OXA-PEG (**B**) and Nio-OXA (**C**) stored at 4 °C and 25 °C over 60 days. **D, E** Stability of Nio-OXA-PEG (**D**) and Nio-OXA (**E**) was assessed through changes in PDI over 60 days. **F, G** Retention of OXA in Nio-OXA-PEG (**F**) and Nio-OXA (**G**) over time at 4 °C and 25 °C. For all charts, ***: $p < 0.001$; **: $p < 0.01$; *: $p < 0.05$ (Mean \pm SD, $n = 3$)

resulting in slower drug diffusion. In comparison with non-PEGylated Nio-OXA, the drug release is further slowed by the addition of polyethylene glycol (PEG) to the Nio-OXA-PEG formulation. In addition to improving stability, PEGylation creates a steric barrier on the niosome surface that lowers the vesicle membrane's permeability and limits the release of encapsulated oxaliplatin. To reduce interactions with surrounding fluids and further restrict premature drug release, PEG chains also form a hydration shell around the niosome. PEGylated formulations extended-release behavior is especially beneficial for the treatment of cancer, since it guarantees longer-lasting medication availability and improved tumor site targeting. Furthermore, by lengthening the

formulation’s bloodstream circulation time and decreasing reticuloendothelial system clearance, PEGylation enhances the formulation’s pharmacokinetics. The rapid initial release seen in the early hours of the study is likely attributable to these surface-associated drug molecules. The gradual diffusion of the medication from inside the niosomal structure accounts for the ensuing extended-release period. This aligns with the expected behavior of niosomes, wherein the surfactant bilayer serves as a controlled release barrier. The heightened bilayer permeability or diminished stability under acidic conditions indicates a more rapid release, perhaps mimicking the tumor microenvironment and enhancing medication release at the necessary site. Generally, the result clearly shows that all formulations showed the second phase of slower release up to 72 h after the initial burst release, which was attributed to OXA diffusion from the outer layer of the niosomes (Rajalakshmi et al. 2018). The encapsulation of oxaliplatin in the niosome could prevent burst release. Moreover, coating oxaliplatin-loaded niosomes with PEG results in a significant reduction in burst release at physiological pH (7.4) (Akbarzadeh et al. 2020a). This trend could be due to being provided a barrier layer for drug diffusion after coating niosomes (Cosco et al. 2009). The accelerated drug release at acidic pH, as opposed to physiological pH, is primarily due to membrane instability, lipid hydrolysis, increased drug solubility, and electrostatic repulsion. Under acidic circumstances, the protonation of surfactant head groups disturbs bilayer structure, hence enhancing membrane fluidity and permeability. Lipid hydrolysis undermines vesicular integrity, resulting in medication leakage. Weakly basic medicines demonstrate heightened ionization in acidic conditions, hence improving their solubility and diffusion from the vesicle (Alemi et al. 2018; Rezaei et al. 2022; Shalviri et al. 2013).

The drug release kinetics of free OXA, naked Nio, Nio-OXA, and PEG-Nio-OXA at different pH were investigated using various kinetic models (Table 6). The value of R2 verified the best model for each formulation. The sample with the highest value of R2 was chosen as the appropriate model for the release mechanism. As can be seen in Table 6, the best-fitting model for pure OXA was the first-order model. However, the

Table 6 Kinetic release models and parameters for niosomal formulations

Release model	Equation	R ²				
		Nio-OXA (pH=7.4–37 °C)	Nio-OXA (pH=5.4–37 °C)	Nio-OXA-PEG (pH=7.4–37 °C)	Nio-OXA-PEG (pH=5.4–37 °C)	Free Oxaliplatin (OXA) (pH=7.4–37 °C)
Zero-order	$C_t = C_0 + K_0t$	R ² =0.80	R ² =0.74	R ² =0.77	R ² =0.77	R ² =0.63
First-order	$\text{Log}C = \text{Log}C_0 + K_1/2.303$	R ² =0.86	R ² =0.84	R ² =0.81	R ² =0.83	R ² =0.97
Higuchi	$Q = K_{Ht} \sqrt{t}$	R ² =0.93	R ² =0.88	R ² =0.90	R ² =0.91	R ² =0.79
Korsmeyer-Peppas	$M_t/M_\infty = K_t n^*$	R ² =0.95 n=0.50	R ² =0.94 n=0.42	R ² =0.94 n=0.54	R ² =0.95 n=0.47	R ² =0.85 n=0.75

This table presents the release kinetics and parameters for free oxaliplatin (OXA), Nio-OXA, and Nio-OXA-PEG formulations under different conditions of pH (7.4 and 5.4) at 37 °C. Various mathematical models were applied to describe the drug release behavior and identify the dominant release mechanisms

* n = Diffusion or release exponent

best model for optimized Nio-OXA and PEG-Nio-OXA formulations at pH=7.4 and pH=5.4 was the Korsmeyer–Peppas model.

Stability

Significant variations between storage conditions (4 °C vs. 25 °C) over time (0, 30, and 60 days) are revealed by the statistical analysis of stability characteristics (Fig. 5B–G). Both Nio-OXA and Nio-OXA-PEG demonstrated a notable increase in vesicle size at 25 °C as opposed to 4 °C, especially at 60 days. Nio-OXA-PEG displayed diameters of 250.9 and 289.3 nm at 4 °C and 25 °C, respectively ($p < 0.001$), whereas Nio-OXA held at 4 °C had an average size of 275.1 nm compared to 324.4 nm at 25 °C ($p < 0.001$). These findings imply that PEGylation offers somewhat improved stability, while higher temperatures encourage vesicle enlargement or aggregation. A lack of regularity in the vesicle size distribution was also shown by the polydispersity index (PDI), which rose noticeably over time and reached greater values at 25 °C. At 60 days, Nio-OXA's PDI was 0.291 at 4 °C and 0.392 at 25 °C ($p < 0.01$), whereas Nio-OXA-PEG's values were 0.266 and 0.315 at 4 °C and 25 °C, respectively ($p < 0.01$). These results emphasize how crucial cold storage is for preserving structural integrity, and PEGylation also improves the stability of the size distribution. The encapsulation efficiency (EE) also declined significantly over time, particularly at 25 °C. At 60 days, Nio-OXA stored at 4 °C retained an EE of 53.21%, while at 25 °C, it dropped to 42.48% ($p < 0.01$). For Nio-OXA-PEG, EE was 61.49% at 4 °C and 54.35% at 25 °C ($p < 0.001$), demonstrating that PEGylation enhances drug retention. Niosomal drug delivery systems can be extended in shelf life and usability through cold storage and PEGylation. Temperature has a major impact on the stability of Nio-OXA and Nio-OXA-PEG formulations due to the niosomes' molecular dynamics and structural integrity. At higher temperatures (25 °C), increased thermal energy promotes molecular mobility, resulting in greater membrane fluidity and instability. This causes vesicle swelling, aggregation, and ultimately drug leakage, as seen by increased vesicle size, increased polydispersity index (PDI), and lower encapsulation efficiency (EE) over time. Furthermore, higher temperatures promote oxidative destruction and hydrolysis of niosomal components including surfactants and cholesterol, jeopardizing structural integrity. At lower temperatures (4 °C), molecular mobility is reduced, minimizing vesicle disruption and preserving the niosome's structural integrity. This explains the much higher stability at 4 °C. Because of its particular features, the addition of polyethylene glycol (PEG) to the niosome formulation improves stability greatly. PEGylation forms a hydrophilic steric barrier on the surface of niosomes, reducing vesicle aggregation and fusion by limiting contacts between nearby vesicles. This steric hindrance serves to maintain uniform vesicle size and slows the rate of size expansion and PDI over time, even at high temperatures. Furthermore, the hydration shell created by PEG lowers the permeability of the vesicle membrane, reducing drug leakage and increasing encapsulation efficiency. PEGylation also improves the vesicles' tolerance to environmental stress, such as temperature-induced membrane breakdown, by stabilizing the lipid bilayer. These effects collectively explain why Nio-OXA-PEG displayed higher stability as compared to Nio-OXA, with a smaller size (Alemi et al. 2018; Safari Sharafshadeh et al. 2024; Mirzaie et al. 2020).

Cytotoxicity

The MTT assay findings indicated that MCF-7 cells treated with pure Nio, free OXA, and PEG-Nio-OXA exhibited reduced cell viability in a dose- and time-dependent pattern. Compared to the control group, free OXA significantly decreased cell viability at 24 h, with levels decreasing to 67% at 50 µg/mL ($p < 0.001$). PEG-Nio-OXA exhibited greater cytotoxicity, reducing cell viability to around 50% ($p < 0.001$), whereas Nio-OXA demonstrated moderate cytotoxicity, decreasing vitality to approximately 60 ($p < 0.001$). Like the untreated control, Pristine Nio exhibited minimal cytotoxicity and kept cell viability above 80%. The cytotoxic effects of all drugs intensified after 48 h. At a concentration of 50 µg/mL, PEG-Nio-OXA exhibited the most significant impact, reducing cell viability to 31%, higher than that of Nio-OXA (about 45%) and free OXA (approximately 62%) ($p < 0.001$). PEG-Nio-OXA surpassed

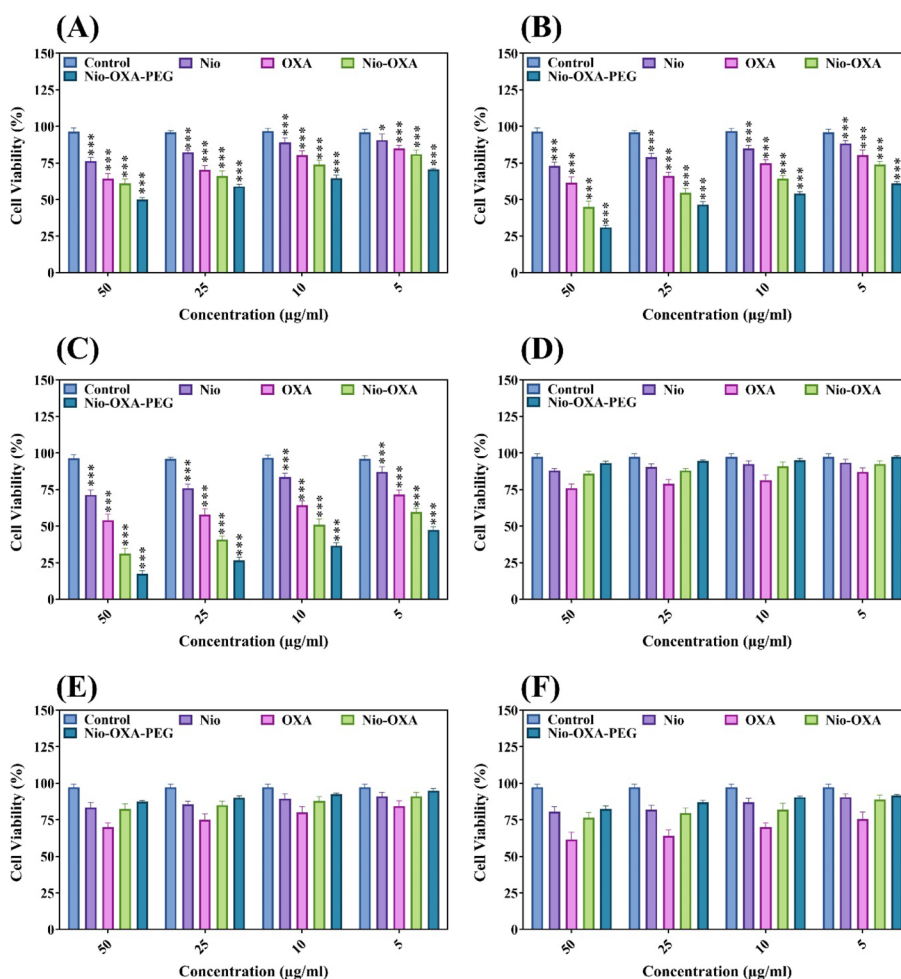


Fig. 6 Cytotoxic effects of control, pristine Nio, free OXA, Nio-OXA, and PEG-Nio-OXA formulations on MCF-7 and HFF cells at different concentrations (50, 25, 10, and 5 µg/mL) over time: **A** Cytotoxicity in MCF-7 cells after 24 h, **B** cytotoxicity in MCF-7 cells after 48 h, **C** cytotoxicity in MCF-7 cells after 72 h, **D** cytotoxicity in HFF cells after 24 h, **E** cytotoxicity in HFF cells after 48 h, and **F** cytotoxicity in HFF cells after 72 h. A dose- and time-dependent decrease in cell viability was observed. Compared to MCF-7 cells, all formulations exhibited lower cytotoxicity in HFF cells. Results are presented as mean ± SD (** $p < 0.05$, *** $p < 0.001$ compared to the control)

all other formulations in decreasing cell viability to below 15% within 72 h ($p < 0.001$). These data illustrate the superior sustained cytotoxicity of PEG-Nio-OXA relative to the control and other formulations (Fig. 6A–C).

HFF cells performed the MTT test to assess off-target toxicity. In comparison with MCF-7 cells, all formulations exhibited significantly reduced cytotoxicity in HFF cells. Cell viability for the control, pure Nio, Nio-OXA, and PEG-Nio-OXA groups remained above 85% after 24 h. At a concentration of 50 $\mu\text{g/mL}$, free OXA marginally reduced viability to about 76%. The administration of Free OXA reduced vitality to around 70% after 48 h, but Nio-OXA and PEG-Nio-OXA maintained viability levels of over 83%. At 72 h, PEG-Nio-OXA exhibited superior biocompatibility, with vitality exceeding 83%, whereas free OXA had the highest off-target toxicity, reducing viability to around 57%. Free OXA exhibited moderate toxicity in HFF cells but rapid cytotoxicity in MCF-7 cells, suggesting non-specific effects. Nio-OXA demonstrated the benefits of encapsulation and controlled release by exhibiting longer cytotoxic effects in MCF-7 cells while exhibiting reduced toxicity in HFF cells. Over all time intervals, PEG-Nio-OXA exhibited the most significant cytotoxic effects on MCF-7 cells, reducing cell viability to below 15% after 72 h. Significantly, it preserved over 85% vitality in HFF cells with few off-target effects. In comparison with the control, PEG-Nio-OXA consistently exhibited the strongest selective cytotoxicity, affirming its promise as a targeted cancer treatment (Fig. 6D–F).

At lower concentrations (e.g., 5 and 10 $\mu\text{g/mL}$), Nio-OXA-PEG consistently reduced cell viability more than Nio-OXA and free OXA. This suggests that PEGylation improves drug transport efficiency and potency, even at inadequate dosages. All formulations showed significantly less cytotoxicity for the HFF cell line, which represents normal fibroblasts than for MCF-7 cells. Nio-OXA-PEG consistently showed the best balance between potent effects on MCF-7 cells and minimal impact on HFF cells, confirming its enhanced selectivity for cancer cells. The inclusion of PEG, which increases stability, lengthens circulation time, and promotes cellular uptake of the medication, is responsible for the increased effects of Nio-OXA-PEG on MCF-7 cells. Increased cytotoxicity results from the hydrophilic PEG layer's reduction of aggregation, improved contact with the cancer cell membrane, and facilitation of drug internalization. Furthermore, the PEGylated formulation's sustained release characteristic guarantees extended drug availability in the tumor microenvironment, optimizing its therapeutic efficacy while lowering systemic toxicity. These findings demonstrate how PEGylation can enhance the effectiveness and selectivity of niosomal drug delivery systems (Safari Sharafshadeh et al. 2024). A possible explanation is that the internalization of Oxaliplatin niosome nanoparticles is enhanced by an endocytosis mechanism of oxaliplatin into cancer cells (Paskeh et al. 2022). These data for HFF indicate that OXA-Nio-PEG cytotoxicity is because of the release of OXA inside the cells, and it is not related to the release of components from empty niosomal formulation (Wiranowska et al. 2020).

Cell cycle

Significant differences between the investigated formulations (Control, pristine Nio, free OXA, OXA-Nio, and PEG-Nio-OXA) on MCF-7 cells over 24, 48, and 72 h are shown by the findings of the cell cycle distribution (Fig. 7A–C). In terms of cell cycle distribution, free OXA considerably raised the sub-G1 population to almost 8% after 24 h, while the

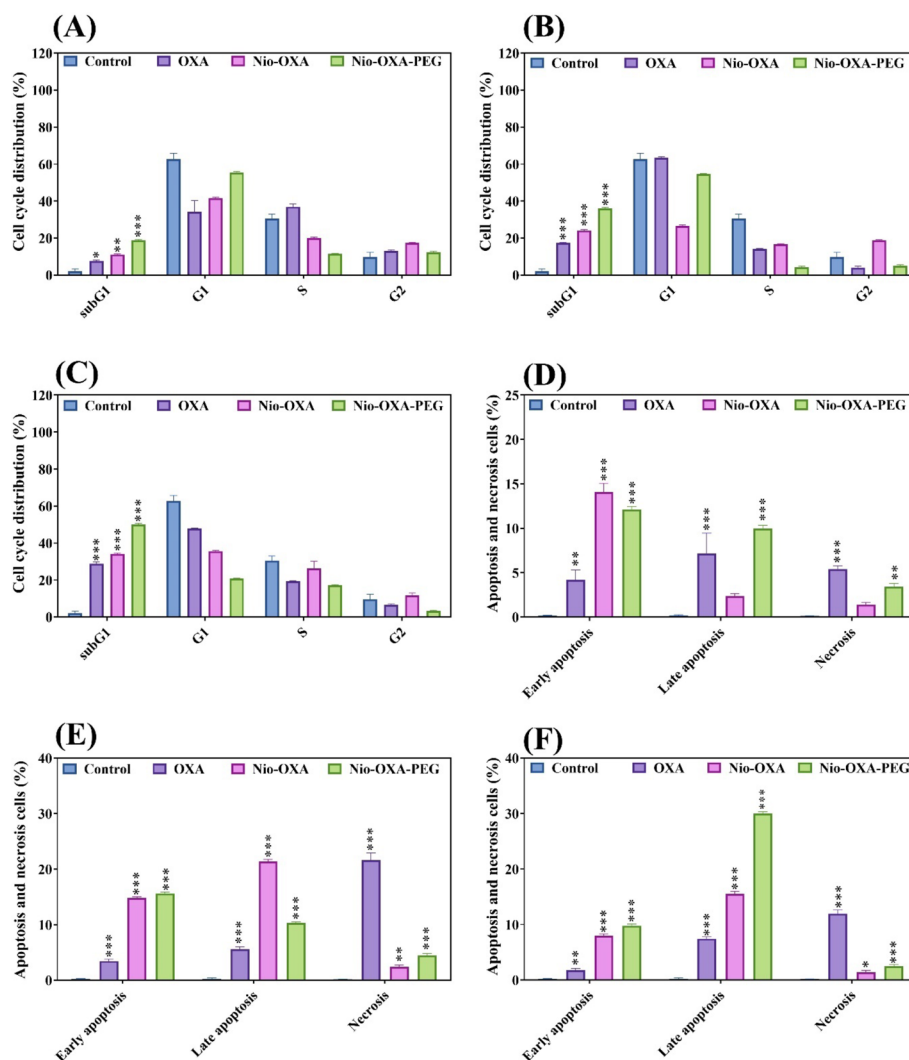


Fig. 7 Effects of control, pristine Nio, free OXA, Nio-OXA, and PEG-Nio-OXA formulations on cell cycle distribution and apoptosis/necrosis in MCF-7 cells: **A** cell cycle distribution after 24 h, **B** cell cycle distribution after 48 h, **C** cell cycle distribution after 72 h, **D** apoptosis and necrosis distribution after 24 h, **E** apoptosis and necrosis distribution after 48 h, and **F** apoptosis and necrosis distribution after 72 h. Data represent the percentage of cells in each phase or apoptotic/necrotic category. Statistical significance is indicated as $**p < 0.05$, $**p < 0.01$, $***p < 0.001$ compared to the control and Data represent means \pm standard deviations ($n = 3$), For all graphs

control group's sub-G1 population stayed below 2% ($p < 0.05$). In addition, the sub-G1 population increased significantly to approximately 10% and 18%, respectively, for Nio-OXA and Nio-OXA-PEG ($p < 0.01$). For both formulations, the sub-G1 population grew even more at 48 h, with Nio-OXA-PEG outperforming Nio-OXA with ~35% compared to ~23% and free OXA reaching ~17% ($p < 0.001$). Free OXA had the smallest sub-G1 population by 72 h (~28%), followed by Nio-OXA-PEG (~50%) and Nio-OXA (~33%). All of these groups were significantly larger than the control group ($p < 0.001$). According to these results, Nio-OXA's cytotoxic capability is increased by PEGylation, which allows it to eventually provide long-lasting apoptotic effects that are on par with or superior to those of free OXA.

Particularly for free OXA, Nio-OXA, and Nio-OXA-PEG, the observed rise in the sub-G1 population suggests severe DNA damage and cell cycle arrest, which results in apoptosis. Because of its immediate drug diffusion and direct contact with DNA, which led to substantial DNA cross-linking and replication inhibition, free OXA induced the fastest increase in the sub-G1 population. On the other hand, the sub-G1 population increased more gradually but steadily over time with the encapsulated formulations, especially Nio-OXA-PEG. This is explained by the niosomal carriers' regulated release of oxaliplatin, which increases drug availability and guarantees long-term cytotoxic action. By increasing the formulation's stability and circulation duration, PEGylation amplifies this effect even more, enabling effective cellular uptake and sustained action. Oxaliplatin's cumulative effects on cell cycle disruption and apoptosis induction are highlighted by the time-dependent rise in the sub-G1 population and apoptotic cells observed in all formulations. Because it was unencapsulated, free OXA had quick cytotoxic effects at earlier timepoints (24 h), but Nio-OXA and Nio-OXA-PEG had longer effects because of their prolonged release patterns.

Flow cytometry

Anticancer medications are essential, because the apoptosis process is responsible for the death of dividing cells. In a current study for further investigation on the antiproliferative effect of free OXA, OXA-Nio, and PEG-Nio-OXA in breast tumor cells, apoptosis was evaluated in MCF-7 cells at 24, 48, and 72 h after treatment by flow cytometry. In addition, we used control samples and untreated cell lines to evaluate them (Fig. 7D–F). In contrast to the control group, which experienced both apoptosis and necrosis at less than 1% ($p < 0.01$), free OXA caused around 4% early apoptosis and 5% necrosis at 24 h. With minimal necrosis, Nio-OXA and Nio-OXA-PEG caused around 1.5% and 3% early apoptosis, respectively, demonstrating that PEGylation increases early apoptotic activity ($p < 0.01$). For free OXA, necrosis stayed below 25% after 48 h, but early apoptosis rose to around 3% and late apoptosis to about 5% ($p < 0.001$). The early apoptosis rates for Nio-OXA and Nio-OXA-PEG were around 14% and 16%, respectively, while the late apoptosis rates were approximately 21% and 10% ($p < 0.01$). Early apoptosis for free OXA peaked at around 2% after 72 h, while necrosis and late apoptosis reached about 11% and 7%, respectively ($p < 0.001$). Among the encapsulated formulations, Nio-OXA-PEG exhibited the highest early apoptosis (~10%), followed by ~30% late apoptosis and ~2% necrosis. These results were comparable to or greater than those of free OXA ($p < 0.001$).

The progressive release of the medication from the niosomal formulations is reflected in this time-dependent behavior, which ensures extended exposure to cancer cells and reduces the possibility of immediate systemic toxicity. The notable increases in early and late apoptosis, especially with Nio-OXA-PEG, demonstrate the apoptotic pathways that the formulations trigger. Through improved contact with the cancer cell membrane, PEGylation increases cellular absorption and facilitates more effective medication internalization. Oxaliplatin interacts with DNA after internalization, initiating apoptotic processes. When compared to free OXA, Nio-OXA-PEG exhibited higher levels of early apoptosis, indicating that PEGylation encourages a better-regulated apoptotic response and lowers the risk of necrotic cell death, which is frequently linked to inflammatory responses. The highest levels of early apoptosis were seen by 72 h, suggesting

that Nio-OXA-PEG is a safer and more effective treatment alternative due to its greater capacity to begin programmed cell death while limiting necrosis. In comparison with Nio-OXA, PEGylation was essential in improving the performance of Nio-OXA-PEG. By enclosing the niosomes in a hydrophilic barrier, the PEG coating increases their durability in biological settings and delays the onset of drug leakage. This increases the therapeutic efficacy of oxaliplatin by guaranteeing a longer and sustained release of the drug. PEG's steric hindrance also increases blood circulation time and decreases nonspecific interactions with healthy cells, enabling more effective accumulation in the tumor microenvironment. This explains why Nio-OXA-PEG showed higher levels of apoptosis and sub-G1 arrest than non-PEGylated formulations, particularly at later time periods (Raymond et al. 2002; Urbanska et al. 2012).

Gene expression

The efficacy of pristine Nio, free OXA, Nio-OXA, and PEG-Nio-OXA to trigger apoptosis and prevent metastasis varies significantly, according to the expression analysis of pro-apoptotic, anti-apoptotic, and metastasis-related genes in MCF-7 cells treated with these formulations (Fig. 8A–C). PEG-Nio-OXA continuously showed the greatest elevation of BAX, Caspase-3, and Caspase-9 for pro-apoptotic markers at all periods. PEG-Nio-OXA raised BAX expression by around 3.5 times ($p < 0.001$) after 24 h, followed by Nio-OXA at 3.0 times ($p < 0.01$) and free OXA at 2.7 times ($p < 0.01$). In comparison with Nio-OXA (3.2-fold) and free OXA (2.4-fold), PEG-Nio-OXA caused a 4.0-fold increase in BAX ($p < 0.001$) after 48 h, and this trend peaked at 5.5-fold at 72 h ($p < 0.001$). Likewise, Caspase-3 and Caspase-9 exhibited maximal expression with PEG-Nio-OXA at all timepoints, peaking at 4.6 and 5.3 at 72 h ($p < 0.001$), with fold changes of 3.3 and 3.0 at 24 h, 3.8 and 3.4 at 48 h. Based on these findings, PEG-Nio-OXA is more efficient than both Nio-OXA and free OXA at triggering apoptotic pathways. On the other hand, PEG-Nio-OXA effectively suppressed survival pathways by significantly downregulating the anti-apoptotic marker BCL2 at all periods, with a fold change of approximately 0.5 at 72 h ($p < 0.01$). In Nio-OXA (~0.6-fold, $p < 0.01$) and free OXA (~0.7-fold, $p < 0.05$), this downregulation was marginally less noticeable. The potential of PEG-Nio-OXA to cause strong and long-lasting apoptosis in cancer cells is highlighted by its capacity to concurrently upregulate pro-apoptotic genes and downregulate anti-apoptotic genes (Safari Sharafshadeh et al. 2024).

PEG-Nio-OXA significantly decreased MMP9 expression (~0.53-fold at 72 h, $p < 0.01$), although free OXA and Nio-OXA showed modest suppression (~0.75-fold and ~0.6-fold, respectively, $p < 0.05$), according to the study of metastasis-related markers, MMP2 and MMP9. Although less impacted, PEG-Nio-OXA nevertheless somewhat decreased MMP2 expression (~0.5-fold, $p < 0.05$), indicating that the PEGylated formulation may be able to prevent tumor invasion and the possibility of metastasis. According to these results, PEG-Nio-OXA inhibits MCF-7 cells' ability to spread by inducing apoptosis. Because PEG-Nio-OXA is PEGylated, which increases stability, prolongs drug release, and promotes cellular uptake, it showed better and longer-lasting effects than free OXA. Although Nio-OXA also showed notable effects, its PEGylated cousin was more successful, demonstrating the crucial role PEG plays in enhancing therapeutic efficacy (Safari Sharafshadeh et al. 2024). The biocompatibility

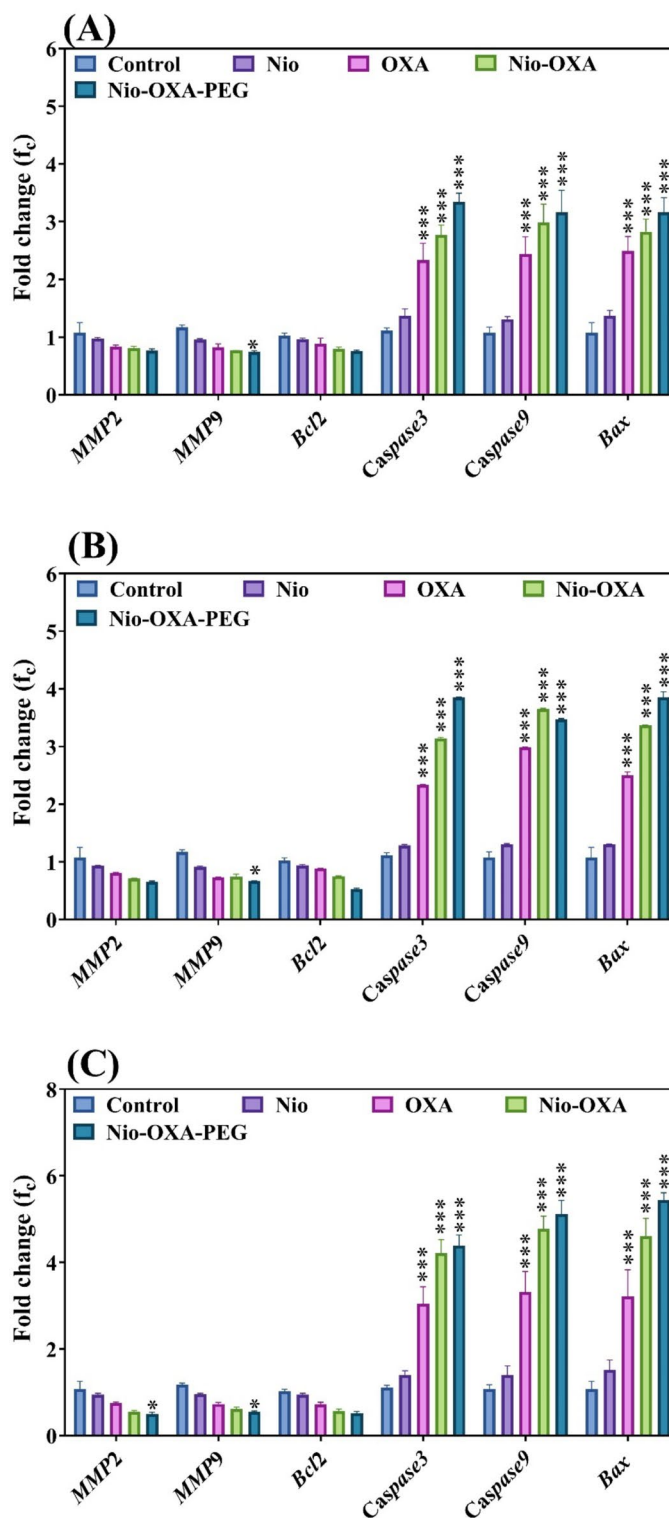


Fig. 8 Expression levels of pro-apoptotic, anti-apoptotic, and metastasis-related genes in MCF-7 cells treated with control, pristine Nio, free OXA, Nio-OXA, and PEG-Nio-OXA: **A** after 24 h, **B** after 48 h, and **C** after 72 h. Fold changes in gene expression are shown for *MMP2*, *MMP9*, *BCL2*, *Caspase-3*, *Caspase-9*, and *BAX*. Results are presented as mean \pm SD, with statistical significance indicated as *** p < 0.001 compared to the control

and non-toxicity of the control and pristine Nio formulations were confirmed by the little changes in gene expression they displayed. The most effective formulation, PEG-Nio-OXA, suppresses anti-apoptotic (BCL2) and metastatic (MMP9) markers while upregulating BAX, Caspase-3, and Caspase-9 to provide strong and prolonged apoptotic activity. These findings highlight its potential as an excellent therapeutic agent for the treatment of cancer, necessitating additional preclinical and clinical testing to verify its safety and effectiveness. Bax is a pro-apoptotic marker that promotes cell death by inducing cytochrome c release from mitochondria (Lindenboim et al. 2024). In this study, both the Nio-OXA and Nio-OXA-PEG significantly upregulated Bax in MCF-7 breast cancer cells. This indicates that the formulations induce apoptosis effectively, contributing to their anticancer activity. While Nio-OXA-PEG showed a higher level of Bax upregulation than Nio-OXA in cancer cells, thus indicating greater pro-apoptotic activity, the improvement in cellular uptake and stability, in addition to their apoptotic activity, is orchestrated according to the latter upregulation on cellular Bax (Nandi et al. 2024). Caspase-3 is a central executioner of apoptosis, in charge of cleaving various substrates within the cell. Nio-OXA and Nio-OXA-PEG induced a significantly higher expression of caspase-3 (Pandey et al. 2024). This elevation indicates the triggering of the apoptotic mechanism, which brings about apoptosis. PEGylated niosomes had a more significant effect, amplifying their efficiency in eradicating cancer cells. In the apoptotic cascade, the initiator caspase that activates downstream caspases, including caspase-3, is caspase-9. Nio-OXA and Nio-OXA-PEG treatments kicked off significantly increased levels of caspase-9 expression. It confirms that both formulations effectively switch on the intrinsic apoptotic pathway (Safari Sharafshadeh et al. 2024; Gupta et al. 2023). The synergistic effect seen in Nio-OXA-PEG indicates that PEGylation may improve oxaliplatin delivery and efficacy in triggering apoptosis. The protein Bcl-2 is an anti-apoptotic marker, and its expression is inhibited by the release of cytochrome c into the cytoplasm (Safari Sharafshadeh et al. 2024; Belka and Budach 2002). The study shows significant downregulation of the expression of Bcl-2 in Nio-OXA and Nio-OXA-PEG-treated cells. The downregulation of Bcl-2 would result in the potentiation of apoptosis and improve the therapeutic effect. The PEGylated niosomes exhibited greater downregulated expressions of Bcl-2, thus indicating that they provoke better apoptotic induction (Safari Sharafshadeh et al. 2024; Salmani-Javan et al. 2023). MMP-2 would degrade the remodeling of the extracellular matrix, promoting cancer cell invasion and ultimately metastasis. MMP-2 was reduced with Nio-OXA treatment and with Nio-OXA-PEG treatment, probably decreasing its metastatic potential. The PEGylated formulation presented a more elaborated reduction of MMP-2 and to some degree would account for its enhanced anticancer properties by restricting cancer cell migration and invasion. In addition to MMP-2, MMP-9 participates in extracellular matrix degradation and the metastasis of cancer. Downregulation of expression of MMP-9 was revealed by the cells treated with the Nio-OXA and Nio-OXA-PEG, suggesting that both formulations could inhibit the invasion of cancer cells. Nio-OXA-PEG was shown to have

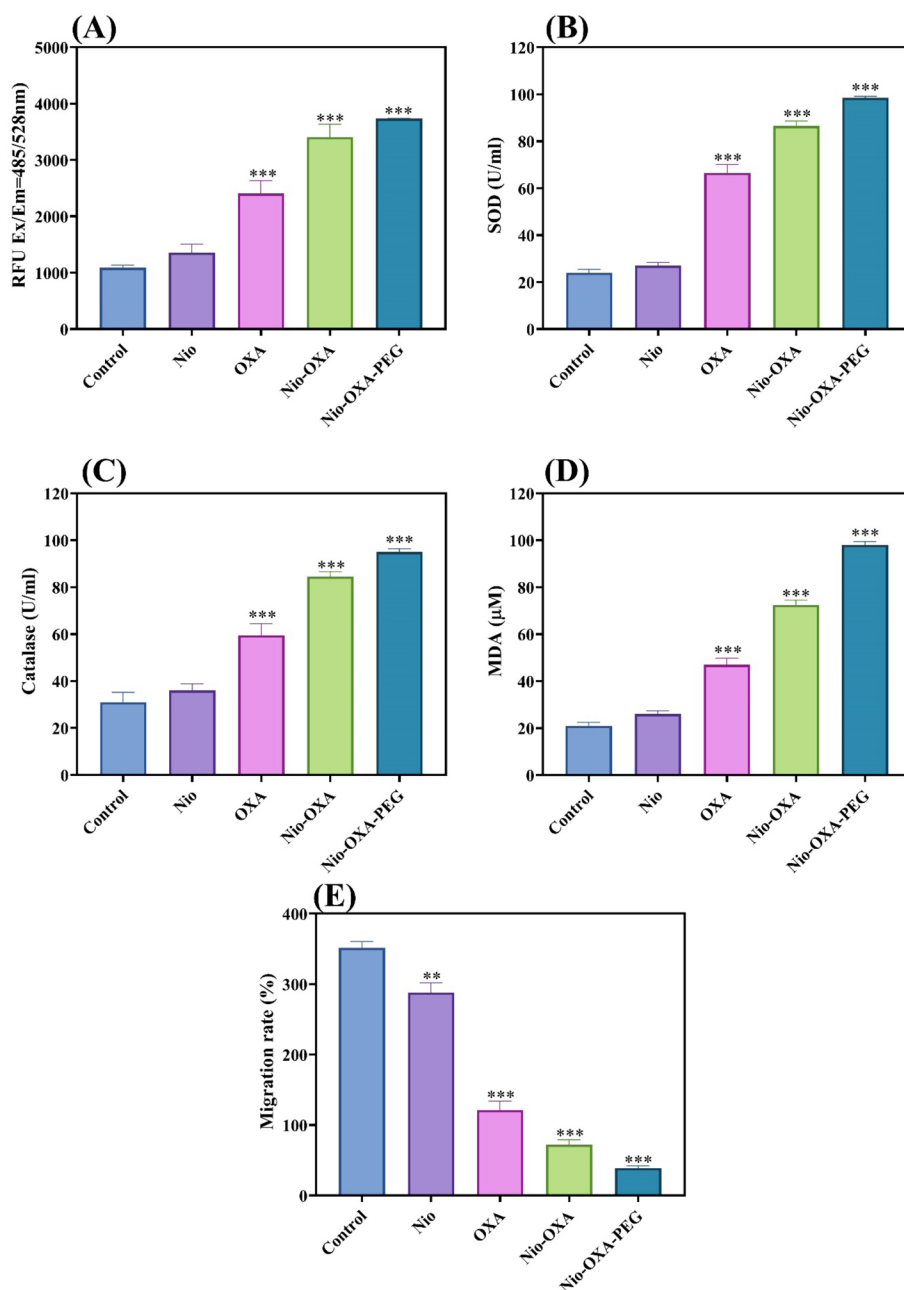


Fig. 9 Analysis of oxidative stress markers, lipid peroxidation, and cell migration in MCF-7 cells treated with control, pristine Nio, free OXA, Nio-OXA, and PEG-Nio-OXA: **A** reactive oxygen species (ROS) levels measured as RFU (Ex/Em: 485/529 nm). ROS levels significantly increased in all treated groups, **B** superoxide dismutase (SOD) activity. SOD activity increased as a defensive response to oxidative stress, **C** catalase activity. The sustained oxidative stress overwhelmed the antioxidant defenses, contributing to apoptosis, **D** malondialdehyde (MDA) levels indicating lipid peroxidation and severe membrane damage, further contributing to cell death, and **E** cell migration inhibition. Results are presented as mean \pm SD, with statistical significance indicated as ** $p < 0.01$, *** $p < 0.001$ compared to the control

enhanced activity than Nio-OXA, indicating the advantage that PEGylation would impart towards therapy using niosomal formulations (Safari Sharafshadeh et al. 2024; Chakrabarti and Patel 2005).

Reactive oxygen species

It seems that one of the most vital features of cell growth is to possess the basic levels of reactive oxygen species (ROS), because extreme levels of ROS stimulate cell death (Gu et al. 2019). In comparison with the control and pure Nio, all treated groups exhibited a considerable increase in reactive oxygen species (ROS) generation (Fig. 9A). Because free OXA can disrupt DNA replication and mitochondrial activity, it caused a significant increase in ROS levels (~ 2400 RFU, $p < 0.001$). Because of the delayed release of oxaliplatin, which prolonged oxidative stress in cancer cells, Nio-OXA displayed a significantly higher ROS level (~ 3400 RFU, $p < 0.001$). PEG-Nio-OXA demonstrated the greatest ROS levels (~ 3700 RFU, $p < 0.001$), highlighting the PEGylated formulation's longer engagement with cancer cells and improved cellular absorption. The higher ROS levels are essential for oxidative damage induction and apoptosis, underscoring PEG-Nio-OXA's enhanced effectiveness in oxidative stress-induced cancer cell death. Significant oxidative stress in MCF-7 cells is indicated by the rise in reactive oxygen species (ROS) levels observed in all treatment groups. The highest ROS levels were elicited by PEG-Nio-OXA (~ 3700 RFU, $p < 0.001$), which is indicative of the PEGylated formulation's improved cellular absorption and extended retention. The increased ROS levels are essential for initiating apoptotic pathways, rupturing mitochondrial membranes, and causing oxidative damage. PEG-Nio-OXA's enhanced therapeutic efficacy can be seen by its ability to induce constant oxidative stress, rendering it a potent carcinogen. ROS can promote apoptosis or necrosis by damaging the DNA, proteins, and lipids of cancer cells. Therefore, the presence of high amounts of ROS leads to cell death. In addition, cancer cells produce more ROS than healthy cells, because they alter oncogene activation, tumor suppressor gene loss, and nuclear and mitochondrial gene expression. As a result, when the level of ROS is low to moderate, it helps cell proliferation, differentiation, and survival. However, the excessive levels of ROS cause cells to die (Joo 2010; Zeng et al. 2016; Yang et al. 2014). Increased ROS levels damage mitochondrial activity, resulting in the release of cytochrome c and the activation of caspase-dependent apoptotic pathways. Furthermore, reactive oxygen species (ROS) interact with lipids, proteins, and nucleic acids, resulting in irreversible damage to cancer cells. PEG-Nio-OXA's capacity to maintain elevated ROS levels indicates persistent oxidative stress, which surpasses the antioxidant defenses of cancer cells, finally resulting in death. In this study, OXA can augment ROS production, and this can produce higher ROS levels in OXA and OXA-Nio treatments (Zhang et al. 2018, 2019; Sundaramoorthy et al. 2016).

Effects on antioxidant status

As compared to the control, the antioxidant enzyme superoxide dismutase (SOD) was markedly elevated in the treated groups (Fig. 9B). Free OXA caused oxidative stress, which raised SOD activity (~ 65 U/mL, $p < 0.001$). Nio-OXA maintained prolonged oxidative stress through sustained drug release, which further increased SOD levels (~ 87 U/mL, $p < 0.001$). With the highest SOD activity (~ 100 U/mL, $p < 0.001$), PEG-Nio-OXA demonstrated the formulation's capacity to produce long-lasting oxidative stress, which forces the cancer cells to strengthen their antioxidant defenses. This finding emphasizes how PEG-Nio-OXA overpowers the antioxidant potential of cells, which in turn encourages oxidative damage. The cells' defensive reaction to increased oxidative stress was

reflected in the considerable increase in superoxide dismutase (SOD) activity observed in all treated groups. Tumor cell proliferation can be affected by SOD enzymes, because they can affect peroxide levels. When the level of SOD overexpresses in human cancer cell lines, the production of H₂O₂ increases and tumor growth reduces in the absence of anticancer agents (Alexandre et al. 2006). The obtained results were in line with the other literature. The level of SOD reduction after UV irradiation is related to the production of many free radicals that surpassed the antioxidant enzymes' scavenging capacity. Moreover, the decrease in enzymatic activity may be attributed to enzyme inactivation brought about by ROS damage to DNA (Ahsanuddin et al. 2016). It has been shown that treatment with drug-loaded niosomes increased the Nrf2 antioxidant signaling pathway (Fadaei et al. 2024).

Catalase activity

Another important antioxidant enzyme, catalase, was markedly elevated in the treated groups (Fig. 9C). The effects of prolonged oxidative stress were reflected in the moderate increase in catalase activity that free OXA caused (~60 U/mL, $p < 0.001$) and the greater levels that Nio-OXA produced (~85 U/mL, $p < 0.001$). Catalase activity was highest in PEG-Nio-OXA (~100 U/mL, $p < 0.001$), which is consistent with its protracted development of oxidative stress. The cancer cells' attempt to detoxify hydrogen peroxide produced during oxidative stress is reflected in the elevated catalase activity. However, this defense mechanism was probably overpowered by PEG-Nio-OXA's continuous ROS generation, which resulted in apoptosis. In treated groups, catalase activity—a gauge of the cell's capacity to detoxify hydrogen peroxide—was noticeably higher. Even if catalase is upregulated, the persistent ROS levels brought on by PEG-Nio-OXA probably surpass the detoxification capacity, which causes oxidative damage and apoptosis to build up. These findings highlight PEGylated formulations' improved capacity to induce oxidative stress, which adds to their higher therapeutic efficacy. The most significant antioxidant defense enzyme in mammalian H₂O₂ detoxifying peroxisomes is catalase. In addition, it can protect cells by controlling hydrogen peroxide (H₂O₂) concentrations (Vetrano et al. 2005; Sedlak and Musatov 2017). Due to mitochondrial defects and a decreased expression of antioxidant enzymes like catalase, tumor cells can produce large amounts of reactive oxygen species (Hu et al. 2005). A possible explanation is that oxaliplatin increased the level of H₂O₂ and the use of catalase decreased the intracellular levels of H₂O₂, which confirms oxaliplatin increases the level of H₂O₂ (Dahan et al. 2009). In addition, CAT activity for the Nio-OXA-PEG was 110 and 60 U/mL.

Malondialdehyde (MDA) determination

A measure of lipid peroxidation, malondialdehyde (MDA), was markedly higher in all treatment groups than in the control (Fig. 9D). While Nio-OXA caused greater levels (~72 μM, $p < 0.001$) because of extended oxidative stress, free OXA displayed intermediate MDA levels (~47 μM, $p < 0.001$). The greatest MDA levels (~100 μM, $p < 0.001$) were seen in PEG-Nio-OXA, suggesting significant oxidative damage to cellular membranes. This finding emphasizes how PEG-Nio-OXA's cytotoxic mechanism includes the induction of lipid peroxidation, which aids in membrane instability and apoptosis.

PEG-Nio-OXA causes widespread lipid peroxidation, which weakens membrane integrity and causes cell death and apoptosis. These results demonstrate that one of the main mechanisms of PEG-Nio-OXA's cytotoxic effects is its capacity to cause oxidative damage.

Elevated MDA levels indicate significant oxidation of lipids, resulting in impaired membrane integrity, diminished membrane potential, and increased permeability. These effects interfere with essential cellular functions, such as ion transport and energy metabolism, accelerating cell death. MDA-induced membrane disruption leads to mitochondrial issues, a critical occurrence in the basic apoptotic cascade. The raised MDA levels associated with PEG-Nio-OXA correspond with increased expression of apoptotic markers, including BAX, Caspase-3, and Caspase-9, indicating that lipid peroxidation plays a crucial role in the formulation's lethal effects. Although free OXA and Nio-OXA elevated ROS and MDA levels, their impact was considerably less substantial than that of PEG-Nio-OXA. Free OXA demonstrated fast although temporary oxidative effects, resulting in small quantities of ROS and MDA. Nio-OXA induced prolonged oxidative stress but did not exhibit the improved cellular absorption and extended circulation duration characteristic of PEGylated formulations. The remarkable efficacy of PEG-Nio-OXA is due to its capacity to produce prolonged oxidative stress and enhance lipid peroxidation, leading to more efficient apoptosis induction. These results show that OXA co-loaded niosomes have a strong oxidative effect on MCF-7 cell lines. Malondialdehyde (MDA) is considered the main product of lipid peroxidation, and it manifests the level of cell damage under oxidation. Therefore, oxaliplatin administration increases nitro-tyrosine, which has been identified as a biomarker of oxidative stress. As a result, the level of MDA increases after treatment with oxaliplatin (Azevedo et al. 2013; Kim et al. 2015).

Cell migration assay

All formulations considerably reduced cell migration (Fig. 9E), a critical component of cancer metastasis, in comparison with the control. Free OXA decreased the migration rate to almost 115% ($p < 0.001$), and Nio-OXA further decreased it to around 75% ($p < 0.001$). The greatest suppression (~40%, $p < 0.001$) was demonstrated by PEG-Nio-OXA, demonstrating its capacity to alter cytoskeletal dynamics and inhibit pathways linked to metastasis. As previously noted, PEG-Nio-OXA's extended release and interaction with metastatic indicators such as MMP9 are responsible for its greater inhibitory effect on cell migration. PEG-Nio-OXA has been shown to downregulate metastasis-related markers, such as MMP9, which is consistent with its increased prevention of migration. These findings imply that PEG-Nio-OXA is a viable anti-cancer agent, since it not only produces cytotoxic effects but also successfully inhibits the potential for metastasis.

Conclusion

For the OXA codelivery, PEGylated Niosome-Based Nanocarriers were successfully designed in this work. Niosomes containing pH-sensitive components, including PEG and Tween, which protonate at lower pH. The prepared functionalized niosomal nanocarriers demonstrated increased stability for 2 months and sustained release at physiological pH. The cytotoxicity of samples enhanced in niosomal formulation

loaded with the drug compared to samples without the drug. In addition, functionalized niosomes resulted in enhancing the cytotoxicity of breast cancer cells. The *in vitro* tests indicated that the oxaliplatin-loaded PEGylate-coated niosomes had noticeable apoptosis in the tested breast cancer cells. The reason why the apoptosis rate increase was due to up/downregulation of the expression of different genes (i.e., *Bax*, *Caspase9*, *Caspase9*, *Bcl-2*, *Bcl2*, *MMP-2*, and *MMP-9*). The antioxidant barrier systems including SOD and catalase, and lipid peroxidation in MCF-7 cell lines raised. Generally, as-designed functionalized niosomal nanocarrier exhibited considerable potential for breast cancer therapy. Particle size, encapsulation efficiency (EE%), stability, and drug-loading capacity are essential formulation factors that must be kept throughout the large-scale production of Oxaliplatin-loaded PEGylated niosomes. The transition of niosomal formulations from laboratory size to bigger batches necessitates careful monitoring of many crucial parameters that may influence product quality characteristics. With suitable changes to process parameters and careful quality control, the shift from small-scale to large-scale manufacturing does not negatively affect EE%, stability, or drug-loading capacity. In addition, Future research must focus on *in vivo* investigations to confirm these findings and develop the significance of this work. Furthermore, investigating long-term impacts and potential therapeutic applications could provide significant findings. These steps will facilitate the connection between experimental findings and practical application.

Supplementary Information

The online version contains supplementary material available at <https://doi.org/10.1186/s12645-025-00309-2>.

Supplementary Material 1.

Acknowledgements

Not applicable for that section.

Author contributions

N.A.M. and A.M. developed the idea and designed the experiments. N.A.M., A.M., F.M., N.A., and H.N.B. conducted the experiments. N.K.F. analyzed the data. N.K.F. wrote the first draft. N.A.M. and A.M. edited the manuscript. All authors confirmed the final manuscript before the submission and agreed to the published version of the manuscript.

Funding

This research did not receive any specific grant from funding agencies in the public, commercial, or not-for-profit sectors and was funded by the authors.

Availability of data and materials

The data generated and/or analyzed during the current study are not publicly available for legal/ethical reasons but are available from the corresponding author upon reasonable request.

Declarations

Ethics approval and consent to participate

Not applicable.

Consent for publication

All authors consent to the publication of this study.

Competing interests

The authors declare no competing interests.

Received: 7 December 2024 Accepted: 10 February 2025

Published online: 05 April 2025

References

- Ahsanuddin S, Lam M, Baron EDJAMS (2016) Skin aging and oxidative stress. *Biomolecules* 3(2):187–195
- Akbarzadeh I, Yaraki MT, Ahmadi S, Chiani M, Nourouzi D (2020a) Folic acid-functionalized niosomal nanoparticles for selective dual-drug delivery into breast cancer cells: an in-vitro investigation. *J Adv Powder Technol* 31(9):4064–4071
- Akbarzadeh I, Saremi Poor A, Yaghmaei S, Norouzi D, Noorbazargan H, Saffar S, Ahangari Cohan R, Bakhshandeh H (2020b) Niosomal delivery of simvastatin to MDA-MB-231 cancer cells. *J Drug Dev Ind Pharm* 46(9):1535–1549
- Akbarzadeh I, Fatemizadeh M, Heidari F, Niri NM (2020c) Niosomal formulation for co-administration of hydrophobic anticancer drugs into MCF-7 cancer cells. *J Arch Adv Biosci* 11(2):1–9
- Akbarzadeh I, Tabarzad M, Khazraei H, Ostovan V (2021) Development of a novel niosomal formulation for Gabapentin. *Iran J Colorect Res* 9(4):149–157
- Alemi A, Zavar Reza J, Haghirsadat F, Zarei Jalilani H, Haghi Karamallah M, Hosseini SA, Haghi Karamallah S (2018) Paclitaxel and curcumin coadministration in novel cationic PEGylated niosomal formulations exhibit enhanced synergistic antitumor efficacy. *J Nanobiotechnol* 16:1–20
- Alexandre J, Nicco C, Chéreau C, Laurent A, Weill B, Goldwasser F, Batteux F (2006) Improvement of the therapeutic index of anticancer drugs by the superoxide dismutase mimic mangafodipir. *J Natl Cancer Inst* 98(4):236–244
- Allen TM, Cullis PR (2013) Liposomal drug delivery systems: from concept to clinical applications. *J Adv Drug Deliv Rev* 65(1):36–48
- Amoozgar H, Ghaffari A, Keramati M, Ahmadi S, Dizaji S, Moayer F, Akbarzadeh I, Abazari M, Bakhshandeh H (2022) A novel formulation of simvastatin nanoemulsion gel for infected wound therapy: In vitro and in vivo assessment. *J Drug Deliv Sci Technol* 72:103369
- André T, Boni C, Navarro M, Taberero J, Hickish T, Topham C, Bonetti A, Clingan P, Bridgewater J, Rivera F (2009) Improved overall survival with oxaliplatin, fluorouracil, and leucovorin as adjuvant treatment in stage II or III colon cancer in the MOSAIC trial. *J Clin Oncol* 27(19):3109–3116
- Arzani G, Haeri A, Daeihamed M, Bakhtiari-Kaboutaraki H, Dadashzadeh S (2015) Niosomal carriers enhance oral bioavailability of carvedilol: effects of bile salt-enriched vesicles and carrier surface charge. *Int J Nanomed* 10:4797
- Azevedo MI, Pereira AF, Nogueira RB, Rolim FE, Brito GA, Wong DVT, Lima-Júnior RC, de Albuquerque RR, Vale ML (2013) The antioxidant effects of the flavonoids rutin and quercetin inhibit oxaliplatin-induced chronic painful peripheral neuropathy. *Mol Pain* 9:1744–8069
- Babaei M, Ardjmand M, Akbarzadeh A, Seyfkhordi A (2014) Efficacy comparison of nanoniosomal and pegylated nanoniosomal Cisplatin on A172 cell line. *J Tissue Eng Regen Med* 11(5):350–354
- Balakrishnan P, Shanmugam S, Lee WS, Lee WM, Kim JO, Oh DH, Kim D-D, Kim JS, Yoo BK, Choi H-G (2009) Formulation and in vitro assessment of minoxidil niosomes for enhanced skin delivery. *Int J Pharm* 377(1–2):1–8
- Baranei M, Taheri RA, Tirgar M, Saeidi A, Oroojalian F, Uzun L, Asefnejad A, Wurm FR, Goodarzi V (2021) Anticancer effect of green tea extract (GTE)-Loaded pH-responsive niosome Coated with PEG against different cell lines. *J Mater Today Commun* 26:101751
- Basiri L, Rajabzadeh G, Bostan A (2017) Physicochemical properties and release behavior of Span 60/Tween 60 niosomes as vehicle for α -Tocopherol delivery. *LWT* 84:471–478
- Belka C, Budach W (2002) Anti-apoptotic Bcl-2 proteins: structure, function and relevance for radiation biology. *Int J Radiat Biol* 78(8):643–658
- Bnyan R, Khan I, Ehtezazi T, Saleem I, Gordon S, O'Neill F, Roberts M (2018) Surfactant effects on lipid-based vesicles properties. *J Pharm Sci* 107(5):1237–1246
- Bourbour M, Khayam N, Noorbazargan H, Yaraki MT, Lalami ZA, Akbarzadeh I, Yeganeh FE, Dolatabadi A, Rad FM, Tan YN (2022) Evaluation of anti-cancer and anti-metastatic effects of folate-PEGylated niosomes for co-delivery of letrozole and ascorbic acid on breast cancer cells. *J Mol Syst des Eng* 7:1102–1118
- Bulbake U, Doppalapudi S, Kommineni N, Khan W (2017) Liposomal formulations in clinical use: an updated review. *Pharmaceutics* 9(2):12
- Chakrabarti S, Patel KD (2005) Matrix metalloproteinase-2 (MMP-2) and MMP-9 in pulmonary pathology. *Exp Lung Res* 31(6):599–621
- Cheng R, Xu T, Wang C, Gan C (2021) The stabilization and antioxidant performances of coenzyme Q10-loaded niosomes coated by PEG and chitosan. *J Mol Liq* 325:115194
- Cosco D, Paolino D, Muzzalupo R, Celia C, Citraro R, Caponio D, Picci N, Fresta M (2009) Novel PEG-coated niosomes based on bola-surfactant as drug carriers for 5-fluorouracil. *J Biomed Microdevices* 11(5):1115–1125
- Dabbagh Moghaddam F, Akbarzadeh I, Marzbankia E, Farid M, Khaledi L, Reihani AH, Javidfar M, Mortazavi P (2021) Delivery of melittin-loaded niosomes for breast cancer treatment: an in vitro and in vivo evaluation of anti-cancer effect. *Cancer Nanotechnol* 12(1):14
- Daeihamed M, Haeri A, Ostad SN, Akhlaghi MF, Dadashzadeh S (2017) Doxorubicin-loaded liposomes: enhancing the oral bioavailability by modulation of physicochemical characteristics. *Nanomedicine* 12(10):1187–1202
- Dahan L, Sadok A, Formento JL, Seitz JF, Kovacic H (2009) Modulation of cellular redox state underlies antagonism between oxaliplatin and cetuximab in human colorectal cancer cell lines. *Br J Pharmacol* 158(2):610–620
- Doi Y, Shimizu T, Ishida Y, Ishida T (2019) Long-term storage of PEGylated liposomal oxaliplatin with improved stability and long circulation times in vivo. *Int J Pharm* 564:237–243
- Duncan B, Kim C, Rotello VM (2010) Gold nanoparticle platforms as drug and biomacromolecule delivery systems. *J Control Release* 148(1):122–127
- Durak S, Esmaeili Rad M, Alp Yetisgin A, Eda Sutova H, Kutlu O, Cetinel S, Zarrabi A (2020) Niosomal drug delivery systems for ocular disease—recent advances and future prospects. *Nanomaterials* 10(6):1191
- Essa EA (2010) Effect of formulation and processing variables on the particle size of sorbitan monopalmitate niosomes. *Asian J Pharm* 4(4):227–233
- Fadaei MS, Fadaei MR, Kheirieh AE, Rahmanian-Devin P, Dabbaghi MM, Tavallaei KN, Shafaghi A, Hatami H, Rahimi VB, Nokhodchi A (2024) Niosome as a promising tool for increasing the effectiveness of anti-inflammatory compounds. *EXCLI J* 23:212

- Gu T, Wang Y, Lu Y, Cheng L, Feng L, Zhang H, Li X, Han G, Liu Z (2019) Platinum nanoparticles to enable electrodynamic therapy for effective cancer treatment. *J Adv Mater* 31(14):1806803
- Gupta J, Abdulsahib WK, Jalil AT, Kareem DS, Aminov Z, Alsaikhan F, Ramirez-Coronel AA, Ramaiah P, Farhood B (2023) Prostate cancer and microRNAs: New insights into apoptosis. *Pathol Res Pract* 245:154436
- Hu Y, Rosen DG, Zhou Y, Feng L, Yang G, Liu J (2005) Huang PJoBC: Mitochondrial manganese-superoxide dismutase expression in ovarian cancer: role in cell proliferation and response to oxidative stress. *J Biol Chem* 280(47):39485–39492
- Joo JH (2010) Jetten AMJCL: Molecular mechanisms involved in farnesol-induced apoptosis. *J Cancer Lett* 287(2):123–135
- Karimifard S, Rezaei N, Jamshidifar E, Moradi Falah Langeroodi S, Abdihaji M, Mansouri A, Hosseini M, Ahmadvani N, Rahmati Z, Heydari M (2022) pH-responsive chitosan-adorned niosome nanocarriers for co-delivery of drugs for breast cancer therapy. *J ACS Appl Nano Mater* 5(7):8811–8825
- Khan DH, Bashir S, Figueiredo P, Santos HA, Khan MI, Peltonen L (2019) Process optimization of ecological probe sonication technique for production of rifampicin loaded niosomes. *J Drug Deliv Sci Technol* 50:27–33
- Kidani Y, Noji M, Tashiro T (1980) Antitumor activity of platinum (II) complexes of 1, 2-diaminocyclohexane isomers. *J GANN Jpn J Cancer Res* 71(5):637–643
- Kim ST, Chung YH, Lee HS, Chung SJ, Lee JH, Sohn UD, Shin YK, Park ES, Kim H-C, Bang JS (2015) Protective effects of phosphatidylcholine on oxaliplatin-induced neuropathy in rats. *J Life Sciences* 130:81–87
- Lindenboim L, Zohar H, Gundersen GG, Worman HJ, Stein R (2024) LINC complex protein nesprin-2 has pro-apoptotic activity via Bcl-2 family proteins. *Cell Death Discov* 10(1):29
- Luciani A, Olivier J-C, Clement O, Siauve N, Brillet P-Y, Bessoud B, Gazeau F, Uchegbu IF, Kahn E, Frija G (2004) Glucose-receptor MR imaging of tumors: study in mice with PEGylated paramagnetic niosomes. *J Radiol* 231(1):135–142
- Luqmani Y (2005) Mechanisms of drug resistance in cancer chemotherapy. *J Med Principles Pract* 14(Suppl. 1):35–48
- Mahdizadeh N, Khorshid Shabestari M, Tafvizi F, Khodarahmi P (2024) Delivery of letrozole-encapsulated niosomes via a 3D bioprinting gelatin–alginate scaffold for potential breast cancer treatment. *Cancer Nanotechnol* 15(1):33
- Maksimov A, Alami M, Zouhiri F, Brion J-D, Pruvost A, Mouglin J, Hamze A, Boissenot T, Provot O, Desmaële D (2014) Therapeutic modalities of squalenoyl nanocomposites in colon cancer: an ongoing search for improved efficacy. *J ACS Nano* 8(3):2018–2032
- Mansoori-Kermani A, Khalighi S, Akbarzadeh I, Niavol FR, Motasadizadeh H, Mahdih A, Jahed V, Abidinezhad M, Rahbari-asr N, Hosseini M (2022) Engineered hyaluronic acid-decorated niosomal nanoparticles for controlled and targeted delivery of epirubicin to treat breast cancer. *J Mater Today Bio* 16:100349
- Mehraya M, Gharehchelou B, Haghghi Poodeh S, Jamshidifar E, Karimifard S, Farasati Far B, Akbarzadeh I, Seifalian A (2022) Niosomal formulation for antibacterial applications. *J Drug Target* 30(5):476–493
- Mirzaie A, Peirovi N, Akbarzadeh I, Moghtaderi M, Heidari F, Yeganeh FE, Noorbazargan H, Mirzazadeh S, Bakhtiari R (2020) Preparation and optimization of ciprofloxacin encapsulated niosomes: a new approach for enhanced antibacterial activity, biofilm inhibition and reduced antibiotic resistance in ciprofloxacin-resistant methicillin-resistance *Staphylococcus aureus*. *J Bioorg Chem* 103:104231
- Miyajima Y, Nakamura H, Kuwata Y, Lee J-D, Masunaga S, Ono K, Maruyama K (2006) Transferrin-loaded nido-carborane liposomes: tumor-targeting boron delivery system for neutron capture therapy. *J Bioconjugate Chem* 17(5):1314–1320
- Moghaddam FA, Ebrahimian M, Oroojalian F, Yazdian-Robati R, Kalalinia F, Tayebi L, Hashemi M (2022) Effect of thymoquinone-loaded lipid–polymer nanoparticles as an oral delivery system on anticancer efficiency of doxorubicin. *J Nanostruct Chem* 12(1):33–44
- Moghtaderi M, Mirzaie A, Zabet N, Moammeri A, Mansoori-Kermani A, Akbarzadeh I, Eshtrati Yeganeh F, Chitgarzadeh A, Bagheri Kashtali A, Ren Q (2021) Enhanced antibacterial activity of *Echinacea angustifolia* extract against multidrug-resistant *Klebsiella pneumoniae* through niosome encapsulation. *J Nanomater* 11(6):1573
- Mohanty D, Rani MJ, Haque MA, Bakshi V, Jahangir MA, Imam SS, Gilani SJ (2020) Preparation and evaluation of transdermal naproxen niosomes: formulation optimization to preclinical anti-inflammatory assessment on murine model. *J Liposome Res* 30(4):377–387
- Nandi S, Nag A, Khatua S, Sen S, Chakraborty N, Naskar A, Acharya K, Calina D, Sharifi-Rad J (2024) Anticancer activity and other biomedical properties of β -sitosterol: Bridging phytochemistry and current pharmacological evidence for future translational approaches. *Phytother Res* 38(2):592–619
- Naseroleslami M, Niri NM, Akbarzade I, Sharifi M, Aboutaleb N (2022) Simvastatin-loaded nano-niosomes confer cardioprotection against myocardial ischemia/reperfusion injury. *J Drug Deliv Transl Res* 12(6):1423–1432
- Pandey S, Jain S, Sahu SK, Gurjar VK, Vaidya A (2024) Caspase-3: a promising target for anticancer agents. *Caspases as molecular targets for cancer therapy*. Elsevier, pp 73–104
- Pando Rodríguez D (2014) Formulation and preparation of niosomes containing bioactive compounds
- Paskeh MDA, Saeifar H, Mahabady MK, Orouei S, Hushmandi K, Entezari M, Hashemi M, Aref AR, Hamblin MR, Ang HL (2022) Overcoming doxorubicin resistance in cancer: siRNA-loaded nanoarchitectures for cancer gene therapy. *J Life Sci* 298:120463
- Rajalakshmi S, Vyawahare N, Pawar A, Mahaparale P, Chellampillai B (2018) Current development in novel drug delivery systems of bioactive molecule plumbagin. *J Artif Cells Nanomed Biotechnol* 46(sup1):209–218
- Raymond E, Faivre S, Chaney S, Woynarowski J, Cvitkovic E (2002) Cellular and molecular pharmacology of oxaliplatin. *J Mol Cancer Ther* 1(3):227–235
- Rezaei T, Rezaei M, Karimifard S, Beram FM, Dakkali MS, Heydari M, Afshari-Behbahani Zadeh S, Mostafaei E, Bokov DO, Ansari MJ (2022) Folic acid-decorated pH-responsive nanoniosomes with enhanced endocytosis for breast cancer therapy: in vitro studies. *J Front Pharmacol* 13:851242
- Riviere K, Kieler-Ferguson HM, Jerger K, Szoka FC Jr (2011) Anti-tumor activity of liposome encapsulated fluoroorotic acid as a single agent and in combination with liposome irinotecan. *J Control Release* 153(3):288–296
- Safari Sharafshadeh M, Tafvizi F, Khodarahmi P, Ehtesham S (2024) Folic acid-functionalized PEGylated niosomes co-encapsulated cisplatin and doxorubicin exhibit enhanced anticancer efficacy. *Cancer Nanotechnol* 15(1):14

- Sahrayi H, Hosseini E, Karimifard S, Khayam N, Meybodi SM, Amiri S, Bourbour M, Farasati Far B, Akbarzadeh I, Bhia M (2021) Co-delivery of letrozole and cyclophosphamide via folic acid-decorated nanoniosomes for breast cancer therapy: synergic effect, augmentation of cytotoxicity, and apoptosis gene expression. *J Pharm* 15(1):6
- Salmani-Javan E, Jafari-Gharabaghloou D, Bonabi E, Zarghami N (2023) Fabricating niosomal-PEG nanoparticles co-loaded with metformin and silibinin for effective treatment of human lung cancer cells. *Front Oncol* 13:1193708
- Sanchez-Munoz A, Perez-Ruiz E, Ribelles N, Marquez A, Alba E (2008) Maintenance treatment in metastatic breast cancer. *J Expert Rev Anticancer Ther* 8(12):1907–1912
- Sedlak E, Musatov A (2017) Inner mechanism of protection of mitochondrial electron-transfer proteins against oxidative damage. Focus on hydrogen peroxide decomposition. *J Biochimie* 142:152–157
- Shalviri A, Chan HK, Raval G, Abdekhodaie MJ, Liu Q, Heerklotz H, Wu XY (2013) Design of pH-responsive nanoparticles of terpolymer of poly (methacrylic acid), polysorbate 80 and starch for delivery of doxorubicin. *J Colloids Surf B Biointerfaces* 101:405–413
- Sundaramoorthy P, Ramasamy T, Mishra SK, Jeong K-Y, Yong CS, Kim JO, Kim HM (2016) Engineering of caveolae-specific self-micellizing anticancer lipid nanoparticles to enhance the chemotherapeutic efficacy of oxaliplatin in colorectal cancer cells. *J Acta Biomaterialia* 42:220–231
- Suzuki R, Takizawa T, Kuwata Y, Mutoh M, Ishiguro N, Utoguchi N, Shinohara A, Eriguchi M, Yanagie H, Maruyama K (2008) Effective anti-tumor activity of oxaliplatin encapsulated in transferrin-PEG-liposome. *Int J Pharm* 346(1–2):143–150
- Tang Z, Meng S, Song Z, Yang X, Li X, Guo H, Du M, Chen J, Zhu YZ, Wang X (2023) Neutrophil membrane fusogenic nanoliposomal leonurine for targeted ischemic stroke therapy via remodeling cerebral niche and restoring blood-brain barrier integrity. *Mater Today Bio* 20:100674
- Trüeb RM (2009) Chemotherapy-induced alopecia. In: *Seminars in cutaneous medicine and surgery: 2009: No longer published by Elsevier*. pp 11–14.
- Urbanska AM, Karagiannis ED, Guajardo G, Langer RS, Anderson DG (2012) Therapeutic effect of orally administered microencapsulated oxaliplatin for colorectal cancer. *J Biomaterials* 33(18):4752–4761
- Vetrano AM, Heck DE, Mariano TM, Mishin V, Laskin DL, Laskin JD (2005) Characterization of the oxidase activity in mammalian catalase. *J Biol Chem* 280(42):35372–35381
- Williams HD, Trevaskis NL, Charman SA, Shanker RM, Charman WN, Pouton CW, Porter CJ (2013) Strategies to address low drug solubility in discovery and development. *J Pharmacol Rev* 65(1):315–499
- Wiranowska M, Singh R, Falahat R, Williams E, Johnson JO, Alcantar N (2020) Preferential drug delivery to tumor cells than normal cells using a tunable niosome–chitosan double package nanodelivery system: a novel in vitro model. *Cancer Nanotechnol* 11(1):1–20
- Wiseman LR, Adkins JC, Plosker GL, Goa KL (1999) Oxaliplatin. *J Drugs Aging* 14(6):459–475
- Yadavar-Nikraves M-S, Ahmadi S, Milani A, Akbarzadeh I, Khoobi M, Vahabpour R, Bolhassani A, Bakhshandeh H (2021) Construction and characterization of a novel tenofovir-loaded pegylated niosome conjugated with tat peptide for evaluation of its cytotoxicity and anti-hiv effects. *J Adv Powder Technol* 32(9):3161–3173
- Yang W, Zou L, Huang C, Lei Y (2014) Redox regulation of cancer metastasis: molecular signaling and therapeutic opportunities. *J Drug Dev Res* 75(5):331–341
- Zeng W, Li Q, Wan T, Liu C, Pan W, Wu Z, Zhang G, Pan J, Qin M, Lin Y (2016) Hyaluronic acid-coated niosomes facilitate tacrolimus ocular delivery: Mucoadhesion, precorneal retention, aqueous humor pharmacokinetics, and transcorneal permeability. *J Colloids Surf B Biointerfaces* 141:28–35
- Zhang Y, Huang L, Shi H, Chen H, Tao J, Shen R, Wang T (2018) Ursolic acid enhances the therapeutic effects of oxaliplatin in colorectal cancer by inhibition of drug resistance. *J Cancer Science* 109(1):94–102
- Zhang P, Shi L, Zhang T, Hong L, He W, Cao P, Shen X, Zheng P, Xia Y, Zou P (2019) Piperlongumine potentiates the antitumor efficacy of oxaliplatin through ROS induction in gastric cancer cells. *J Cel Oncol* 42(6):847–860

Publisher's Note

Springer Nature remains neutral with regard to jurisdictional claims in published maps and institutional affiliations.